Graduate School ETD Form 9
(Revised 12/07)

PURDUE UNIVERSITY
GRADUATE SCHOOL
Thesis/Dissertation Acceptance

This is to certify that the thesis/dissertation prepared

By Chang Jiang

Entitled Signaling Pathways Involved in Mechanical Stimulation and ECM Geometry in Bone Cells

For the degree of Master of Science in Biomedical Engineering

Is approved by the final examining committee:

Hiroki Yokota
Chair

Yunlong Liu

Julie Ji

To the best of my knowledge and as understood by the student in the *Research Integrity and Copyright Disclaimer (Graduate School Form 20)*, this thesis/dissertation adheres to the provisions of Purdue University's "Policy on Integrity in Research" and the use of copyrighted material.

Approved by Major Professor(s): Hiroki Yokota

Approved by: John H. Schild (Head of the Graduate Program) June 11, 2010 (Date)

Graduate School Form 20
(Revised 1/10)

PURDUE UNIVERSITY
GRADUATE SCHOOL

Research Integrity and Copyright Disclaimer

Title of Thesis/Dissertation:
Signaling Pathways Involved in Mechanical Stimulation and ECM Geometry in Bone Cells

For the degree of Master of Science in Biomedical Engineering

I certify that in the preparation of this thesis, I have observed the provisions of *Purdue University Teaching, Research, and Outreach Policy on Research Misconduct (VIII.3.1)*, October 1, 2008.*

Further, I certify that this work is free of plagiarism and all materials appearing in this thesis/dissertation have been properly quoted and attributed.

I certify that all copyrighted material incorporated into this thesis/dissertation is in compliance with the United States' copyright law and that I have received written permission from the copyright owners for my use of their work, which is beyond the scope of the law. I agree to indemnify and save harmless Purdue University from any and all claims that may be asserted or that may arise from any copyright violation.

CHANG JIANG
Printed Name and Signature of Candidate

06/11/2010
Date (month/day/year)

*Located at http://www.purdue.edu/policies/pages/teach_res_outreach/viii_3_1.html

SIGNALING PATHWAYS INVOLVED IN MECHANICAL STIMULATION AND ECM GEOMETRY IN BONE CELLS

A Thesis
Submitted to the Faculty
of
Purdue University
by
Chang Jiang

In Partial Fulfillment of the
Requirements for the Degree
of
Master of Science in Biomedical Engineering

August 2010
Purdue University
Indianapolis, Indiana

ACKNOWLEDGMENTS

I would like to acknowledge my major advisor Dr. Hiroki Yokota for his guidance, support and encouragement to me during the process of this research. Dr. Yokota not only introduced me to the world of biology and guided me in research, but also serves as a role model for me due to his meticulous and passionate attitude towards science.

I would like to thank my advisor committee member Dr. Yunlong Liu for the guidance on microarray analysis, the generous help in usage of software in his lab, and for the tremendous support to my family.

I would like to thank my advisory committee member and my friend Dr. Julie Ji for reading this thesis and the great help and encouragement she has given to me.

I would like to extend my acknowledgement to my amazing colleagues: Dr. Hideyuki Hirasawa, without whose help I could not have finished this study on time; Dr. Ping Zhang, who did a wonderful job in the animal study; and Dr. Kazunori Hamamura, who provided valuable preliminary data for this study.

I would like to thank Wai-Sei Valerie Lim for her help on thesis formatting.

I would like to thank Frank Smith for his help in editing this thesis.

Special thanks to my husband Mingxiang Teng for his incredible support to my career as well as for his assistance on microarray analysis.

TABLE OF CONTENTS

Page

Page

LIST OF TABLES

LIST OF FIGURES

Figure Page

Figure Page

Figure Page

LIST OF ABBREVIATIONS

2D	2-dimensional
3D	3-dimensional
ALP	alkaline phosphatase
ATF3	activating transcription factor 3
ATF4	activating transcription factor 4
ATF6	activating transcription factor 6
BSP	bone sialoprotein
CDK2	cyclin-dependent kinase 2
CHOP	C/EBP homologous protein
Col I	type I collagen
DMP1	dentin matrix protein 1
ECM	extracellular matrix
eIF2α	eukaryotic initiation factor 2, subunit α
ER	endoplasmic reticulum
ERK	extracellular signal-regulated protein kinase
FAK	focal adhesion kinase
FBS	fetal bovine serum
GAPDH	glyceraldehydes-3-phosphate dehydrogenase
IRE1	inositol-requiring protein-1
MAPK	mitogen-activated protein kinase
MEM	minimum essential medium
MSCs	mesenchymal stem cells
OCN	osteocalcin
Osx	osterix
PCR	polymerase chain reaction
Perk	protein kinase RNA-like ER kinase
PI3K	phosphatidylinositol-3 kinase
Re	Reynolds number
siRNA	small interfering RNA
Tg	thapsigargin
Tn	tunicamycin
UPR	unfolded protein responses
Xbp1	X-box binding protein 1

ABSTRACT

Jiang, Chang. M.S.B.M.E., Purdue University, August 2010. Signaling Pathways Involved in Mechanical Stimulation and ECM Geometry in Bone Cells. Major Professor: Hiroki Yokota.

The proliferation and differentiation of osteoblasts are influenced by mechanical and geometrical growth environments. A specific aim of my thesis was the elucidation of signaling pathways involved in mechanical stimulation and geometric alterations of the extracellular matrix (ECM). A pair of questions addressed herein was (a) Does mechanical stimulation modulate translational regulation through the phosphorylation of eukaryotic initiation factor 2α (eIF2α)? (b) Do geometric alterations affect the phosphorylation patterns of mitogen-activated protein kinase (MAPK) signaling? My hypothesis was mechanical stress enhances the proliferation and survival of osteoblasts through the reduction in phosphorylation of eIF2α, while 3-dimensional (3D) ECM stimulates differentiation of osteoblasts through the elevation of phosphorylation of p38 MAPK.

First, mechanical stimulation reduced the phosphorylation of eIF2α. Furthermore, flow pre-treatment reduced thapsigargin-induced cell mortality through suppression of phosphorylation of protein kinase RNA-like ER kinase (Perk). However, H_2O_2-driven cell mortality, which is not mediated by Perk, was not suppressed by mechanical stimulation. Second, in the ECM geometry study, the expression of the active (phosphorylated) form of p130Cas, focal adhesion kinase (FAK) and extracellular signal-regulated protein kinase (ERK) was reduced in cells grown in the 3D matrix. Conversely,

phosphorylation of p38 MAPK was elevated in the 3D matrix and its up-regulation was linked to an increase in mRNA levels of dentin matrix protein 1 and bone sialoprotein.

In summary, our observations suggest the pro-survival role of mechanical stimulation and the modulation of osteoblastic fates by ECM geometry.

1. INTRODUCTION

1.1 Objective and Background

The objective of my thesis is to elucidate the role of mechanical stimulation and ECM geometry in the proliferation and differentiation of osteoblasts. Two specific aims are:

- Aim 1: Examine the effects of varying cellular stresses such as mechanical stimulation, stress to the endoplasmic reticulum and oxidation on translational regulation through eIF2α.

- Aim 2: Evaluate the effects of environmental alterations, in particular ECM geometry, in osteoblastic development.

In Aim 1, an integrated stress response within cells can be caused by a number of insults including hypoxia, nutrient deprivation, viral infection, oxidation and stress to the endoplasmic reticulum (ER) [1-3]. That stress response leads to preferential translational activation by a mechanism involving phosphorylation of eIF2α [4]. In the case of extreme levels of insults the response leads to apoptosis [5]. Although mechanical stimulation increases anabolic responses in bone tissue [6-8] and reduces TNFα driven cell death [9], little is known about load-driven transcriptional and translational regulation mediated by phosphorylation of eIF2α.

In Aim 2, the alteration of ECM is treated as a unique form of cellular stress. Skeletal tissues are responsive to alterations in ECM and capable of adjusting their structural and functional integrity through a process called remodeling [10]. ECM in bone

offers a track for cellular migration and a communication link for cell-cell interactions and multiple types of cells such as osteocytes, osteoclasts and osteoblasts act synergistically for remodeling of ECM. Osteoblasts are primarily responsible for synthesizing and depositing ECM molecules such as type I collagen, bone sialoprotein (BSP) and dentin matrix protein 1 (DMP1) [11]. To actively control the fate of osteoblasts and promote wound healing or organ reconstruction, the effects of various stimulators including chemical agents such as ascorbic acid [12], growth hormones such as PTH [13] and mechanical loading [14] have been investigated. Little is known, however, about the role of ECM milieu in osteoblastic development.

The present study was designed to examine: (a) effects of various stresses on phosphorylation of eIF2α and cell mortality; and (b) role of ECM milieu in osteoblastic development. The following sets of specific questions were posed:

1. Does mechanical stimulation (*in vivo* loading and *in vitro* fluid flow treatment) modulate phosphorylation of eIF2α? If yes, what eIF2α kinase is responsible for? Does fluid flow treatment of osteoblasts suppress stress-driven cell mortality?

2. Do alterations of ECM milieu change genome-wide signaling pathways? If yes, are those pathways involved in the interactions with ECM molecules or osteoblastic mineralization?

Regarding Aim 1, previous studies have shown that thapsigargin, a pharmacological inducer of stress to the ER, alters expression of transcription factors such as ATF4, Runx2 and Osterix in MC3T3 osteoblast-like cells [15]. Since Perk, one of the four known eIF2α kinases, is responsive to ER mediated stress [16], we hypothesized that mechanical stimulation to bone would alter phosphorylation of eIF2α through Perk and affect cell mortality. Regarding Aim 2, the elevation of alkaline phosphatase activity is reported in adult human osteoblasts grown in native collagen gels [17]. It is

hypothesized in the current study that a 3D culture would activate molecular pathways that suppress cellular proliferation and promote osteoblastic differentiation.

To examine the hypotheses in Aim 1, we evaluated the protein expression levels of eIF2α and its phosphorylated form in mouse ulnae, primary mesenchymal stem cells (MSCs) and MC3T3 cells under various stress conditions. The ulnae were loaded with an elbow loading modality [18], while the MSCs and MC3T3 cells were treated with 1 h fluid flow at 20 dynes/cm^2. Focusing on the MC3T3 cells, the mRNA and protein levels of the selected stress-linked genes were determined and cell mortality was evaluated in the presence and the absence of mechanical stimulation, the stressors to the ER (thapsigargin and tunicamycin) or an oxidative agent (H_2O_2) [19-20]. Gene expression was determined by quantitative real-time PCR and Western blot analysis, and the role of Perk was examined by depleting its mRNA with small interfering RNA (siRNA).

To examine the hypotheses in Aim 2, we undertook a genome-wide gene expression analysis using MC3T3 E1 osteoblast-like cells that were grown on a collagen-coated dish (2D model) or seeded in a collagen matrix (3D model). We first predicted molecular signaling pathways that were linked to differential gene expression in the 2D and 3D models, and then examined their potential roles in osteoblast differentiation through a series of real-time PCR and Western analyses. Signaling pathways were analyzed using PathwayExpress software, while the prediction of transcriptional factor binding motifs was conducted using custom-made software. In order to evaluate the mRNA-based prediction in a proteome level, we examined phosphorylation patterns of the selected proteins linked to cellular proliferation and differentiation. Those proteins include a docking protein (p130Crk-associated substrate-p130Cas) [21] and 4 kinases such as focal adhesion kinase (FAK) [22], extracellular signal-regulated protein kinase 1/2 (ERK1/2) [23] and p38 mitogen-activated protein kinase (p38 MAPK) [24]. The role of p38 MAPK in promoting osteoblast differentiation was verified using its selective inhibitor – SB203580 [25].

1.2 Organization of the Thesis

The present thesis is divided into 5 chapters.

- Chapter 1: Introduction including the specific aims, questions and hypotheses.
- Chapter 2: Materials and Methods, and Results of Aim 1 (study on mechanical stimulation and other cellular stresses).
- Chapter 3: Materials and Methods, and Results of Aim 2 (study on ECM geometry and signaling pathways).
- Chapter 4: Discussion of the results in Aims 1 and 2 including significance to human health care, the limitation of current studies and potential future directions.
- Chapter 5: Summary and conclusions.

2. MECHANICAL STIMULATION SUPPRESSES PHOSPHORYLATION OF EIF2α THROUGH PERK IN RESPONSE TO ER STRESS

This study investigated the role of mechanical stimulation in the regulation of eIF2α and cell death. Mechanical stimulation was applied to mouse ulnae, MC3T3 cells and mesenchymal stem cells. Our hypothesis was that mechanical stimulation to bone would alter phosphorylation of eIF2α through Perk and affect cell mortality. To examine this hypothesis, we employed two flow shear systems. Agents such as thapsigargin and H_2O_2 were used to induce cell mortality, and siRNA technology was applied to silence a specific kinase: Perk. A series of western analysis and real time PCR experiments were conducted.

2.1 Materials and Methods

2.1.1 Elbow Loading

Using C57/BL6 mice (female, ~ 12 weeks; Harlan Sprague-Dawley, Inc.), elbow loading was conducted with the procedure described previously [18]. In brief, the mouse was anesthetized and loads were applied to the left elbow for 3 min in the lateral-medial direction with 0.5 N force at 5 Hz. The right forelimb was used as a contralateral control. The pairs of ulnae were harvested at 1, 3 and 5 h after loading. Soft surrounding tissues were dissected out. The bone sample was ground with a mortar and pestle in a RIPA lysis buffer and centrifuged at 4ºC. The supernatant was used for Western blot analysis.

2.1.2 Cell Culture

MC3T3 osteoblast-like cells (C4 clone) were cultured on a glass slide coated with 40 μg/ml type I collagen (BD Biosciences) in αMEM containing 10% fetal bovine serum (FBS) and antibiotics (50 units/ml penicillin and 50 μg/ml streptomycin) [26]. To establish primary MSC culture, femurs and tibias were collected from 4 to 8 week old C57/BL6 mice. Using a 21-gauge needle, bone marrow cells were harvested with Iscove's MEM (Gibco-invitrogen) containing 2% FBS [27-28]. Mononuclear cells were separated by low density gradient centrifugation. Cells were then washed twice with Iscove's MEM and cultured in mouse MesenCult basal medium supplemented with MesenCult Supplemental (Stem Cell Technologies Inc.).

2.1.3 Treatment of Cells

Cellular stress was induced by incubating cells with either 1 μM thapsigargin (Tg, Santa Cruz Biotech.) for 1 - 24 h, 1 μg/ml tunicamycin (Tn, MP Biomedicals) for 3 h, or 0.5 - 2 mM hydrogen peroxide (H_2O_2, Fisher Scientific) for 3 or 6 h. The flow pre-treatment was applied for 1 h at 20 dynes/cm^2 shear stress. Note that this shear stress is relevant to the loading force employed in the *in vivo* model [29]. Prior to flow application, cells were grown for 1 day in a medium containing 1% FBS. For examination of cell mortality, cells were stained with trypan blue and the numbers of live and dead cells were counted separately using a hemacytometer.

2.1.4 Fluid Flow Systems

2.1.4.1 Chamber Flow System

Two fluid flow systems (the chamber flow system and shaker flow system) were employed. The chamber flow system used a Streamer Gold flow device (Flexcell International) depicted in Figure 2.1. The flow chamber contains six slots into which

glass slides with cells can be placed. The flow reservoir was filled with 180 ml cell culture medium, and the whole system was placed into a standard cell culture incubator with an environment of 37ºC and 5% CO_2 [30].

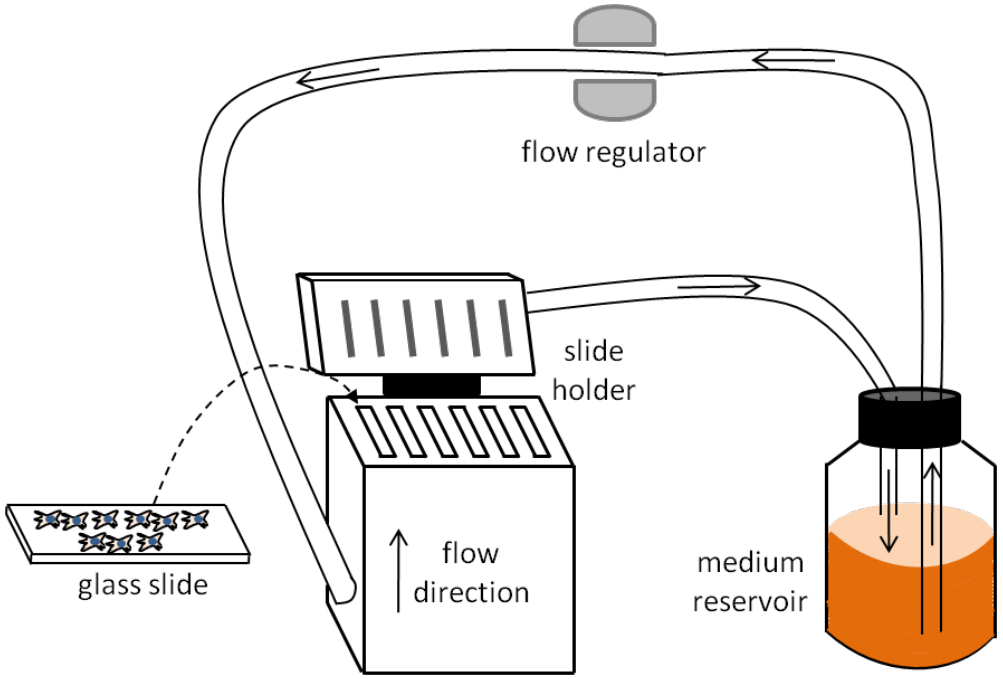

Figure 2.1 Schematic of the chamber flow system

In this system, the medium flow was constrained by a pair of stationary parallel plates and a Poiseuille flow was driven by a pressure gradient as shown in Figure 2.2.

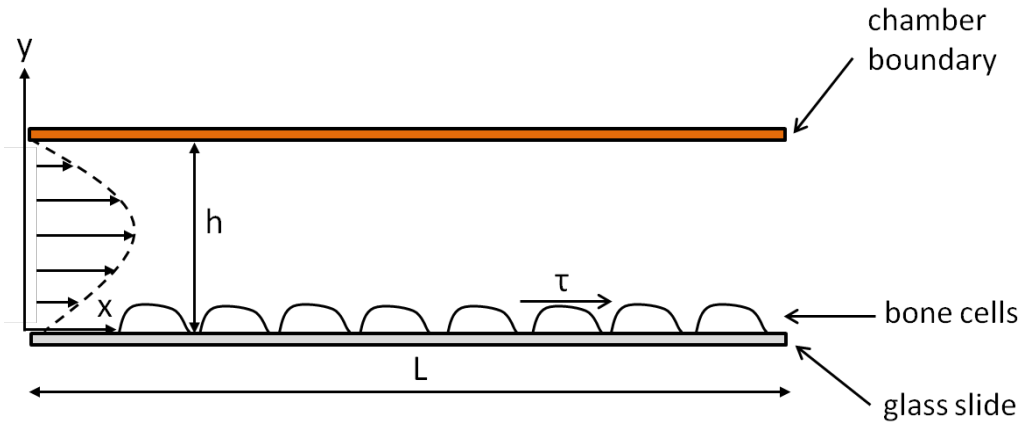

Figure 2.2 Poiseuille flow in the chamber flow system: medium flows from high to low pressure, exerting shear stress on the slide's surface in the flow direction

The shear stress on the flow chamber can be calculated:

$$\tau = \mu \frac{\partial u}{\partial y} \tag{2.1}$$

where μ = dynamic viscosity of the fluid, u = velocity of the fluid along the boundary, and y = height of the boundary. For a Plane Poiseuille flow model, the Navier-Stokes equation was simplified:

$$\frac{d^2u}{dy^2} = \frac{1}{\mu}\frac{dp}{dx} \tag{2.2}$$

in which p = pressure, and x = coordinate along the flow direction. Shear stress τ is thus estimated:

$$\tau = \frac{dp}{dx}\left(y - \frac{h}{2}\right) \tag{2.3}$$

where h = separating distance between the two parallel boundaries. Deducing from a momentum balance for a Newtonian fluid,

$$\tau = \frac{6Q\mu}{wh^2} \quad (2.4)$$

in which Q = volumetric flow rate, and wh = the cross section area of the slots in the chamber. The wall shear stress τ is then determined. The Reynolds number for this system is:

$$Re = \frac{VL\rho}{\mu} = \frac{QL\rho}{\mu w h} \quad (2.5)$$

where V = mean fluid velocity, L = travelled length of medium, and ρ = medium density. When Q is in the range of 0 - 1700 ml/min in the current study, Re is less than 2000. Thus, the fluid flow in the chamber is laminar and the shear stress calculation above is valid. With this system, shear stress in the range of 2 to 45 dynes/cm^2 was induced.

2.1.4.2 Shaker Flow System

In the shaker flow system, illustrated in Figure 2.3, the cell covered glass slides were placed in a rotating flow consisting of 30 ml cell culture medium.

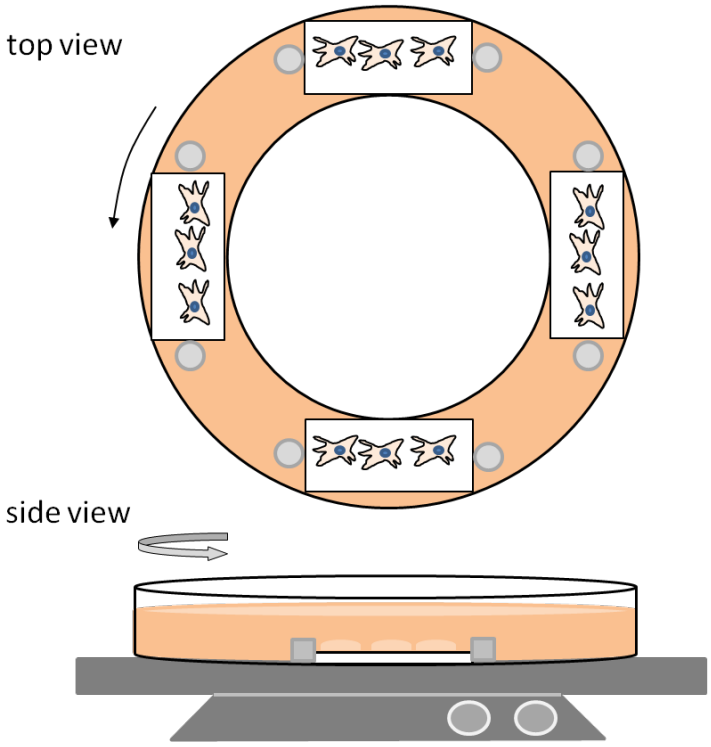

Figure 2.3 Schematic of the shaker flow system

The Reynolds number of this system is calculated:

$$Re = \frac{VL}{v} = \frac{r\omega L}{v} \tag{2.6}$$

where L = length of the glass slides, r = mean radius of the medium flow, ω = angular velocity of fluid flow, and v = kinematic viscosity of the medium.

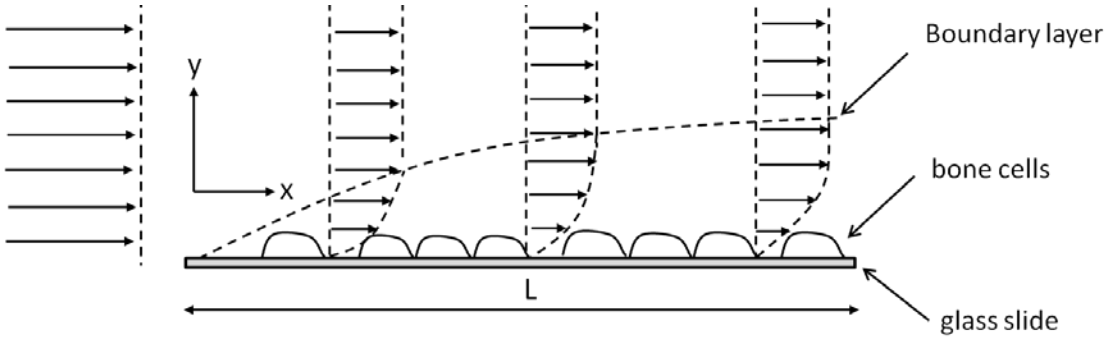

Figure 2.4 Boundary layer in the shaker flow system: medium flows uniformly except in a boundary layer that grows along the length of a glass slide

For the system at 30 rpm, Re is 8,600 (laminar when Re < 500,000). Using the Blasius equation for a laminar flow, shear stress on the glass slides is estimated:

$$\tau = \frac{0.332\rho V^2\sqrt{v}}{\sqrt{Vx}} = \frac{0.332\rho(rw)^{\frac{3}{2}}}{\sqrt{x}}\sqrt{v} \tag{2.7}$$

where V = fluid velocity at infinity, and x = coordinate along the flow direction. When Integrating τ along the slide length L, the stress becomes:

$$\tau = \int_0^L \frac{0.332\rho(rw)^{\frac{3}{2}}}{\sqrt{x}}\sqrt{v} = \frac{0.664\rho(rw)^{\frac{3}{2}}}{\sqrt{L}}\sqrt{v} \tag{2.8}$$

We employed shear stress of 2 - 5 dynes/cm^2 at 30 - 50 rpm.

2.1.4.3 Comparisons Between the Chamber Flow System and the Shaker Flow System

To verify predicted stress values induced by the two systems (chamber and shaker flow systems), the expression levels of two stress response genes (c-fos and ATF4) were determined. Using the chamber flow system, a series of shear stress including 2, 5, 20 and 45 dynes/cm^2 were applied. For the shaker flow system, 30 and 50 rpm rotation

speeds were employed. After 1 h fluid flow, RNA was isolated and reverse transcription followed by real-time PCR was conducted.

2.1.5 Real-time PCR

The mRNA levels of ATF3, ATF4, ATF6, CHOP, c-fos and Xbp1 in response to Tg and/or flow were determined using quantitative real-time PCR with the primers listed in Table 2.1. Total RNA was extracted using an RNeasy Plus mini kit (Qiagen). Reverse transcription was performed, and real-time PCR was carried out using ABI 7500 with SYBR green PCR kits (Applied Biosystems). The mRNA level of GAPDH was used as an internal control to calibrate potential variations in cell numbers. Within the four experimental groups (control, flow alone, Tg alone and flow followed by Tg), the relative mRNA levels of the selected genes were determined with respect to the GAPDH mRNA levels. The results were analyzed using a ΔC_T method [15], in which mRNA levels were normalized by setting the levels in the control group to 1. For analysis of Xbp1 splicing, PCR products were separated on a 2.5% agarose gel and ethidium bromide stained bands were captured using a Fujifilm Luminescent image analyzer (LAS-3000). Note that the expected Xbp1 mRNA sizes were 289 bp (unspliced) and 263 bp (spliced).

Table 2.1 Real-time PCR primers for the mechanical stimulation study

Gene	Forward primer	Backward primer
ATF3	5’-CGAAGACTGGAGCAAAATGATG-3’	5’-CAGGTTAGCAAAATCCTCAAATAC-3’
ATF4	5’-TGGCGAGTGTAAGGAGCTAGAAA -3’	5’- TCTTCCCCCTTGCCTTACG -3’
ATF6	5’-GGATTTGATGCCTTGGGAGTCAGAC-3’	5’-ATTTTTTTCTTTGGAGTCAGTCCAT-3’
CHOP	5’-CCACCACACCTGAAAGCAGAA -3’	5’- GGTGCCCCCAATTTCATCT -3’
Perk	5’-CCGTGACCCATCTGCACTAAT-3’	5’-CATAAATGGCGACCCAGCTT-3’
Xbp1	5’-TTACGGGAGAAAACTCACGGC-3’	5’-GGGTCCAACTTGTCCAGAATGC-3’
GAPDH	5’- TGCACCACCAACTGCTTAG -3’	5’- GGATGCAGGGATGATGTTC -3’

2.1.6 Immunoblots

Cells were sonicated using a sonic dismembrator (Model 100, Fisher Scientific) and lysed in a RIPA lysis buffer containing protease inhibitors (Santa Cruz Biotech) and

phosphatase inhibitors (Calbiochem). Isolated proteins were fractionated using 8 - 12% SDS gels and electro-transferred to Immobilon-P membranes (Millipore). Immunoblots were carried out using antibodies specific to ATF4, eIF2α, Perk, phospho-Perk (Thr980), caspase-3 (total and cleaved forms; Cell Signaling); CHOP (Santa Cruz); phospho-eIF2α (pS^{52}) (Biosource) and β-actin (Sigma). After incubation with anti-rabbit IgG (Cell Signaling) or anti-mouse IgG (Amersham) antibodies conjugated with HRP, signals were detected with ECL chemiluminescence. Images were captured using a Fujifilm Luminescent image analyzer and analyzed using Adobe Photoshop (version 7.0).

2.1.7 RNA Interference

To evaluate the role of Perk in Tg-induced stress with and without the flow pre-treatment, cells were treated with siRNA specific to Perk. In brief, Perk siRNA (sc-36214, Santa Cruz Biotech.) was mixed with a siRNA transfection reagent (sc-36868) in a transfection medium (sc-36868), and the mixture was incubated with cells for 18 h without FBS and antibiotics. Control siRNA-A (sc-37007) was employed as the siRNA control. The Perk mRNA level was evaluated by real-time PCR using the pair of primers included in Table 2.1. Transfected cells were used for experiments after growing in a normal αMEM medium for 2 days.

2.1.8 Statistical Analysis

All values are expressed as mean ± S.D. Data were evaluated using Fisher's PLSD post hoc test after one-way ANOVA tests with Stat View 5.0 (SAS Institute). Statistical significance was examined at $p < 0.05$. Note that statistical significance was indicated in figures with * ($p < 0.05$), ** ($p < 0.01$) and *** ($p < 0.001$).

2.2 Results

2.2.1 Comparisons of Messenger RNA Levels Using the Two Flow Systems

We chose ATF4 and c-fos as two stress responsive genes in osteoblasts, since their RNA expression levels altered depending on shear intensities. In Figure 2.5, a linear regression analysis was conducted to establish the relationships between the induced mRNA expression levels and estimated shear stress intensities.

In the shaker system, the ATF4 mRNA levels were increased 1.1-fold (30 rpm) and 1.25-fold (50 rpm) of those of the control cells. The c-fos mRNA expression levels were elevated by 1.35 and 2.75 times at 30 rpm and 50 rpm respectively. Note that all the data were the average of the results generated from experiments replicated at least once.

The two linear regression lines, generated for ATF4 and c-fos with the chamber flow system, provided a "reference curve" for estimating shear intensities with the shaker flow system. Consequently, the rotations at 30 and 50 rpm induced shear stress equivalent to 2 and 5 dynes/cm^2 with the chamber flow system respectively. This experiment based estimation was in congruity with the estimation obtained from the Blasius equation.

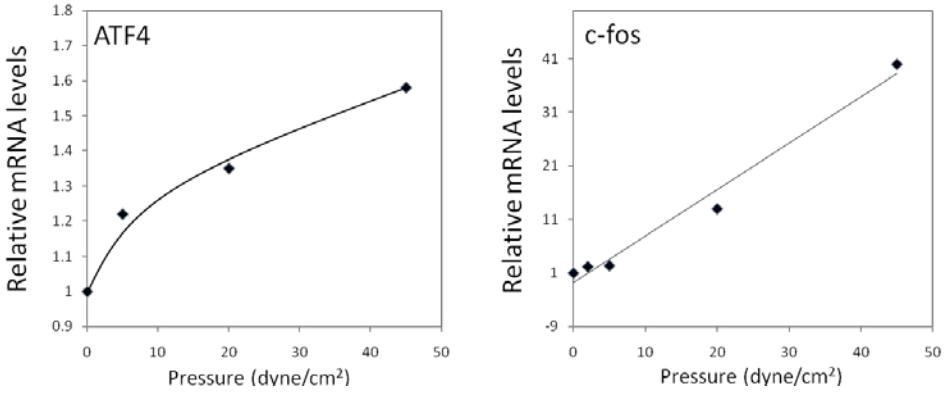

Figure 2.5 Relative mRNA levels of ATF4 and c-fos of MC3T3 cells in response to a series of shear stress generated by the chamber flow system

2.2.2 Load-driven Down-regulation of eIF2α-p *In Vivo* and *In Vitro*

Mechanical stimulation reduced the phosphorylated level of eIF2α (eIF2α-p) (Figure 2.7). First, the loaded ulnae exhibited a lower level of eIF2α-p than the contralateral counterpart with no alteration in the level of eIF2α. Second, in response to flow treatment, the level of eIF2α-p decreased in both MSCs and MC3T3 cells. Figure 2.6 shows the experimental time scheme for *in vitro* fluid flow treatment by the chamber flow system.

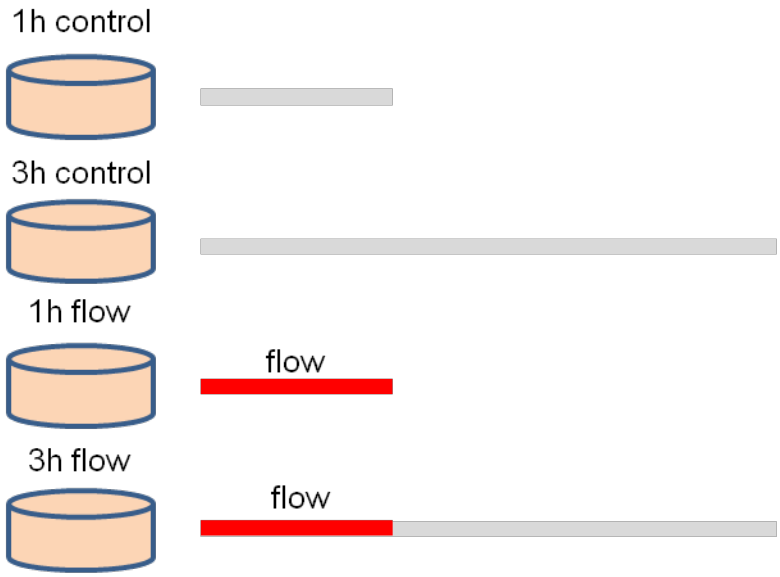

Figure 2.6 Experimental time scheme for *in vitro* fluid flow treatment

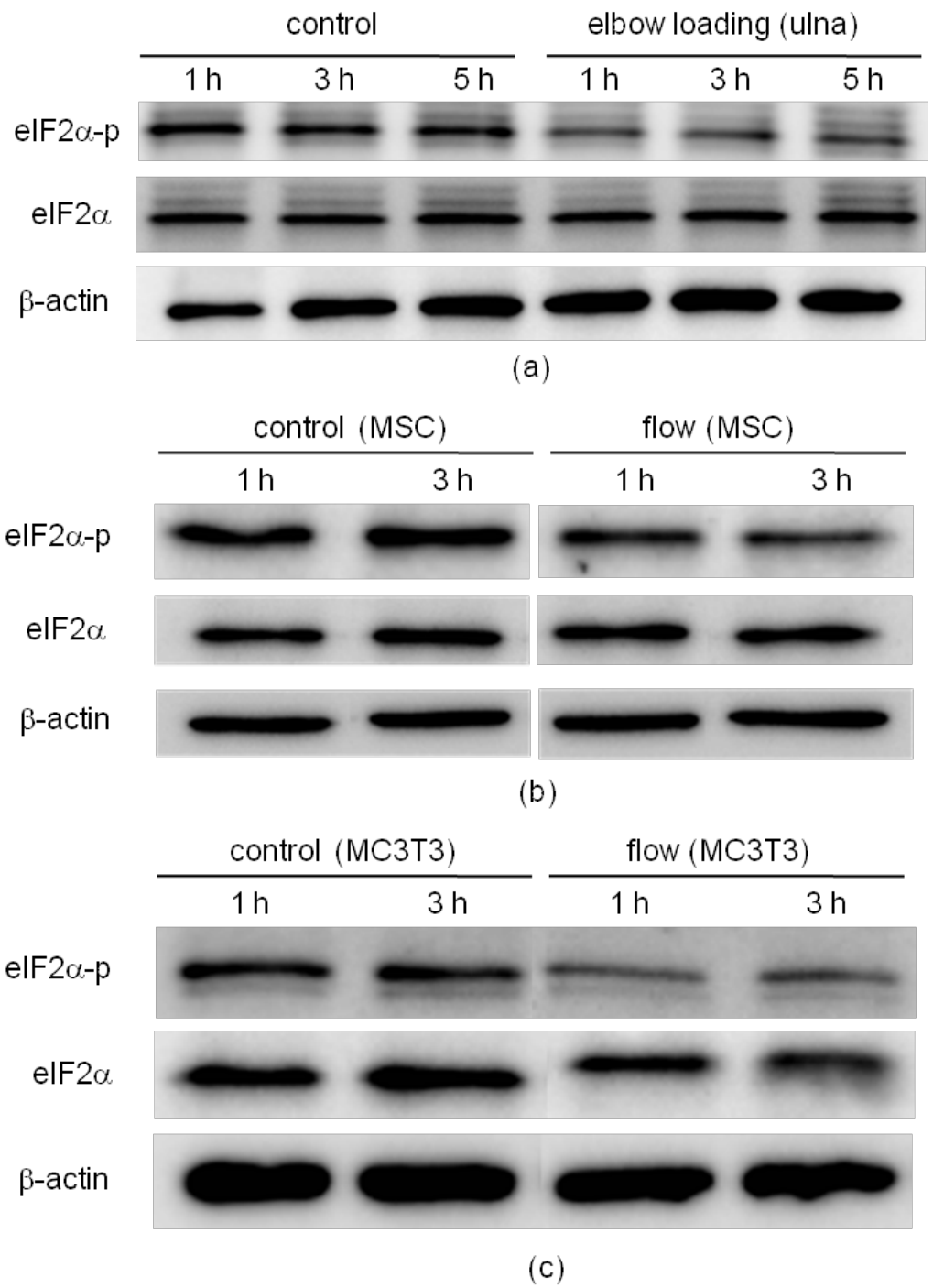

Figure 2.7 Load-driven down-regulation of eIF2α phosphorylation. (a) Reduction in eIF2α-p in the loaded ulnae. (b) Reduction in eIF2α-p in MSCs. (c) Reduction in eIF2α-p in MC3T3 cells

2.2.3 Alterations in the Protein Levels of Perk-p

In concert with load-driven down-regulation of eIF2α-p, mechanical stimulation reduced the level of phosphorylated Perk (Perk-p) in the mouse ulnae (Figure 2.9). Since the basal expression level of Perk-p was low, we confirmed the effects of mechanical stimulation on the expression levels of Perk-p in the presence of ER stress inducers (1 μM Tg and 1 μg/ml Tn) in MC3T3 cells. Figure 2.8 shows the time scheme of this experiment. First, Tg elevated the Perk-p levels as well as the levels of a pro-apoptotic gene: CHOP. However, the 1 h flow pre-treatment suppressed their elevation by 31% (Perk-p) and 49% (CHOP). Second, the flow pre-treatment reduced Tn-driven up-regulation of eIF2α-p, Perk-p and CHOP by 20%, 22% and 75%, respectively. Note that the levels of ATF4 protein were up-regulated by Tg and Tn, and the levels of Perk were unchanged in all cases.

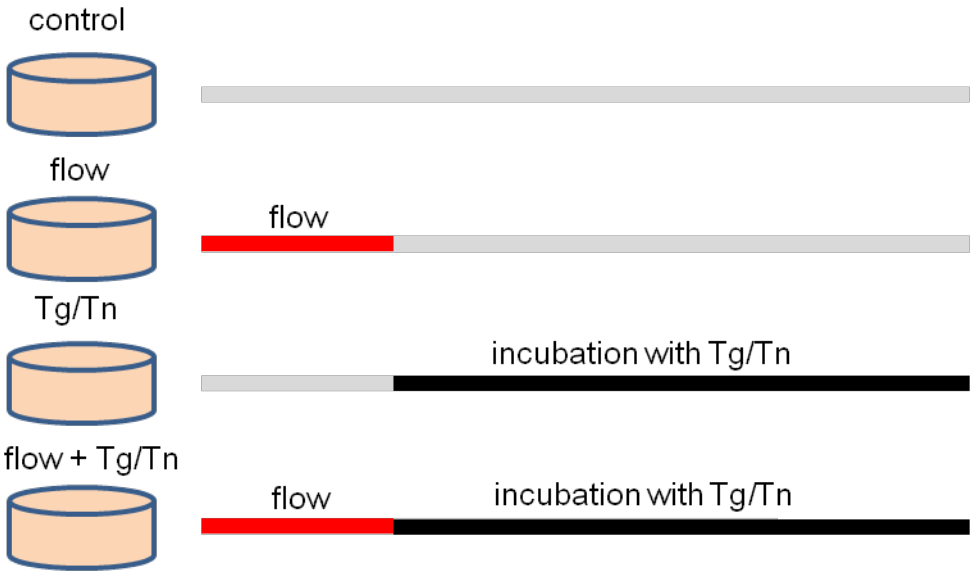

Figure 2.8 Experimental time scheme for *in vitro* fluid flow in combination with Thapsigargin (Tg)/Tunicamycin (Tn) treatment

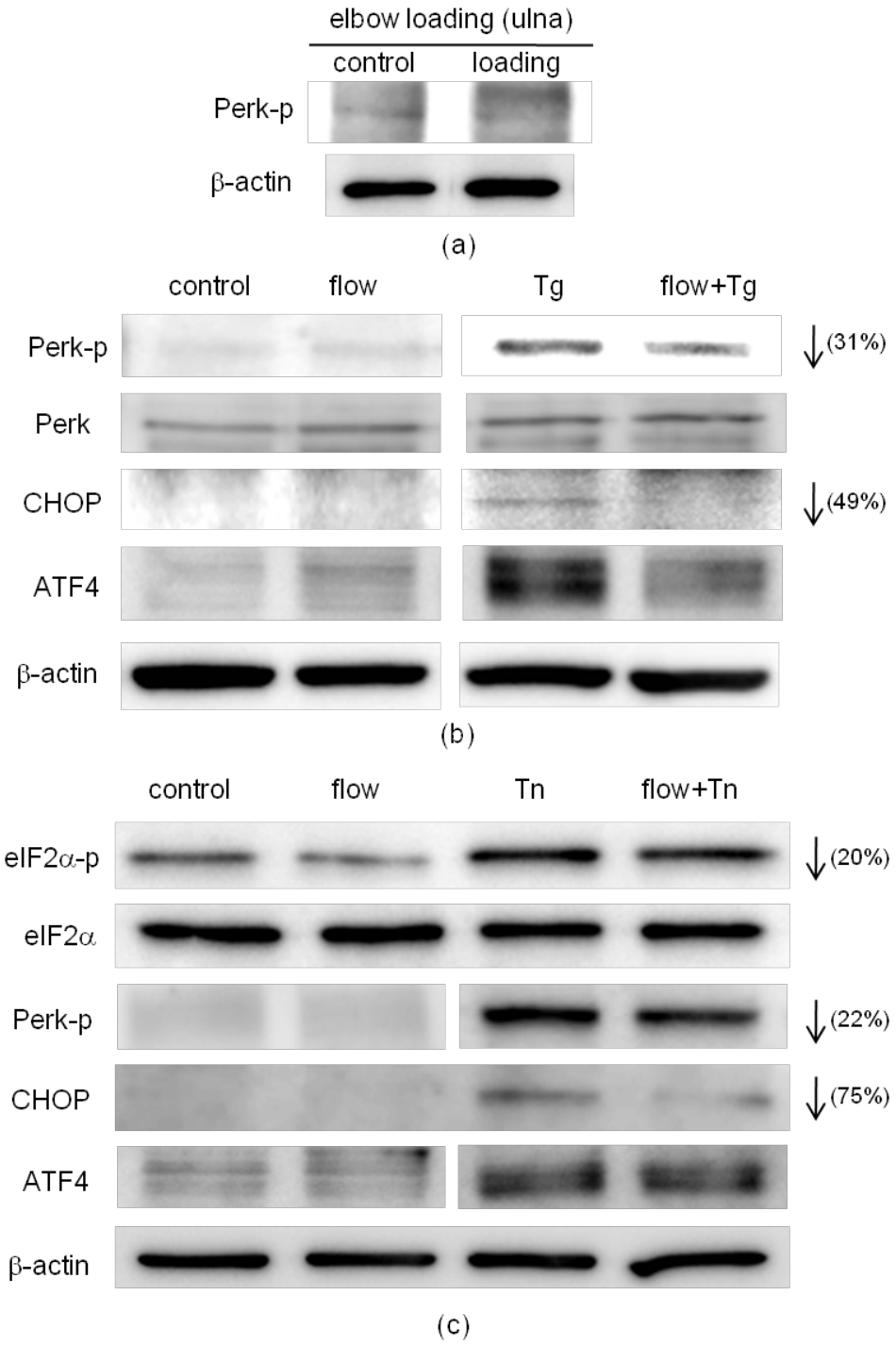

Figure 2.9 Decreased protein levels of Perk-p, CHOP and ATF4 in response to mechanical stimulation. (a) Reduction in Perk-p in the loaded ulnae. (b) Suppression of Tg-driven increases in Perk-p, CHOP and ATF4 by 1 h flow in MC3T3 cells. Cells were incubated with 1μM Tg for 3 h. (c) Suppression of Tn-driven increases in eIF2α-p, Perk-p and CHOP by 1 h flow in MC3T3 cells. Cells were incubated with 1μg/ml Tn for 3 h

2.2.4 Messenger RNA Expression of Xbp1, ATF3, ATF4, ATF6 and CHOP

Expression and splicing of Xbp1 are known to be sensitive to stress to the ER. We examined the effects of Tg and flow pre-treatment on the total Xbp1 mRNA levels and two splicing isoforms. First, 1h incubation with Tg elevated the Xbp1 mRNA levels approximately 2-fold regardless of the flow pre-treatment (Figure 2.10 (a)). Second, additional incubation for 2 h in the presence of Tg increased mRNA levels (14-fold increase) but flow pre-treatment significantly reduced Tg-driven increase (Figure 2.10 (b)). Third, the electrophoretic agarose gel showed that Tg stimulated the splicing of Xbp1 mRNA (Figure 2.10 (c)). Flow pre-treatment reduced the levels of spliced Xbp1 mRNA.

We next examined the mRNA levels of 4 other genes (ATF3, ATF4, ATF6 and CHOP), which are known to be responsive to stress to the ER (Figure 2.10 (d) - (g)). In the absence of Tg, their mRNA levels were not significantly affected by the flow pre-treatment. However, Tg elevated all of the mRNA levels. Flow pre-treatment did not affect the levels of ATF3 mRNA or ATF4 mRNA but suppressed Tg-driven mRNA increases of ATF6 ($p < 0.01$) and CHOP ($p < 0.05$).

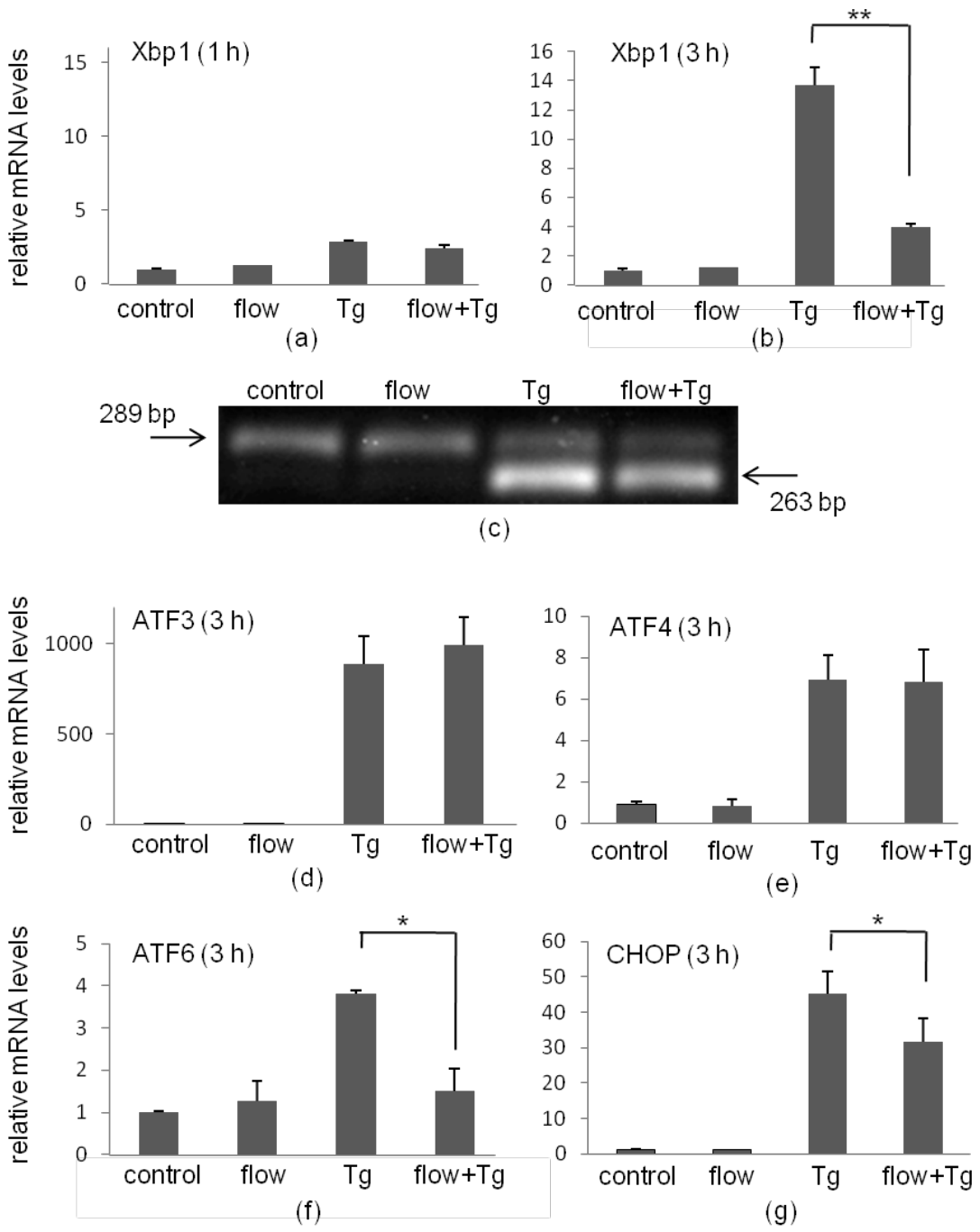

Figure 2.10 Relative mRNA levels of Xbp1, ATF3, ATF4, ATF6 and CHOP in response to Tg and/or mechanical stimulation in MC3T3 cells. (a) Relative Xbp1 mRNA levels after 1 h incubation with Tg. (b) Relative Xbp1 mRNA after 3 h incubation with Tg. (c) Gel images showing the spliced and the unspliced Xbp1 mRNAs after 3 h incubation with Tg. (d) - (g) Messenger RNA levels of ATF3, ATF4, ATF6 and CHOP after 3 h incubation with Tg

2.2.5 Effects of Tg with and without Fluid Flow on Cell Mortality

To investigate a potential effect of mechanical stimulation on cell mortality, cells were incubated with Tg for 24 h with and without 1 h flow pre-treatment generated by shaker flow system (Figure 2.11). First, Tg increased the mortality rate from 3% to 23%, and this increase was suppressed to 10% by 1 h flow pre-treatment (Figure 2.12 (c)). Second, the level of the cleaved isoform of caspase 3, which was undetectable in control regardless of flow treatment (data not shown), was elevated by Tg. In agreement with observations of flow-driven reduction in cell mortality, 1 h flow pre-treatment suppressed this Tg-induced caspase 3 (cleaved) level by 39% (Figure 2.12 (d)).

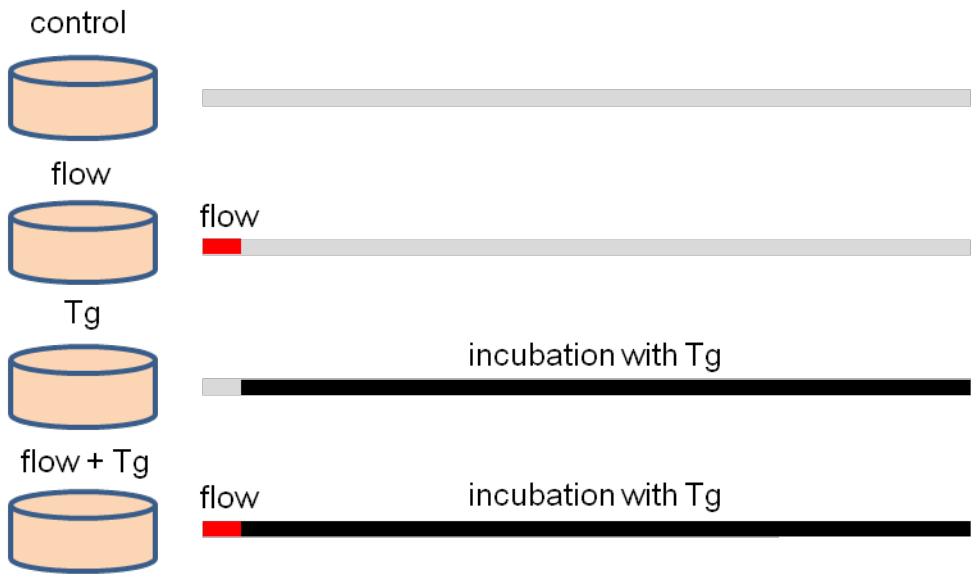

Figure 2.11 Experimental time scheme for cell mortality study by Tg with and without fluid flow treatment

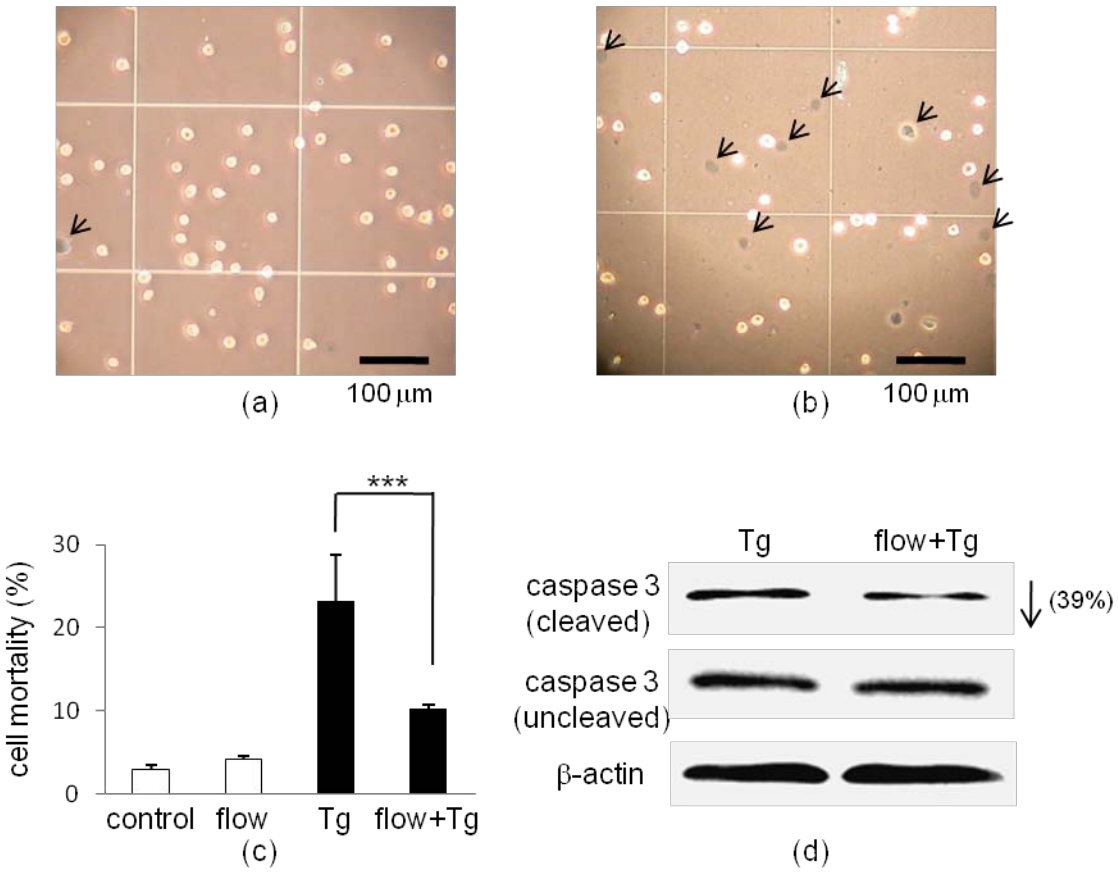

Figure 2.12 Cell mortality in response to 1 μM Tg for 24 h with and without flow pre-treatment in MC3T3 cells. (a) Trypan blue stained control cells. (b) Trypan blue stained cells treated with Tg. (c) Cell mortality (in %) in 4 experimental groups (control, flow alone, Tg alone and Tg preceded by flow). (d) Caspase 3 expression (cleaved and uncleaved isoforms) for the cells incubated with Tg

2.2.6 Effects of Oxidative Stress on Cell Mortality

Since oxidative stress by H_2O_2 also induces an integrated stress response, a potential role of the flow pre-treatment in H_2O_2 induced regulation of eIF2α was examined. First, the flow pre-treatment did not significantly alter the number of dead cells in response to 3 or 6 h incubation with 0.5, 1 or 2 mM H_2O_2 (Figure 2.13 (a) - (b)). Second, Western blot analysis revealed that although administration of H_2O_2 up-regulated eIF2α-p, phosphorylation of Perk was not activated (Figure 2.13 (c)). Furthermore, the

flow pre-treatment did not alter levels of eIF2α-p. These results indicate that efficacy of mechanical stimulation in alleviating cell mortality depends on the stress source and activation of Perk.

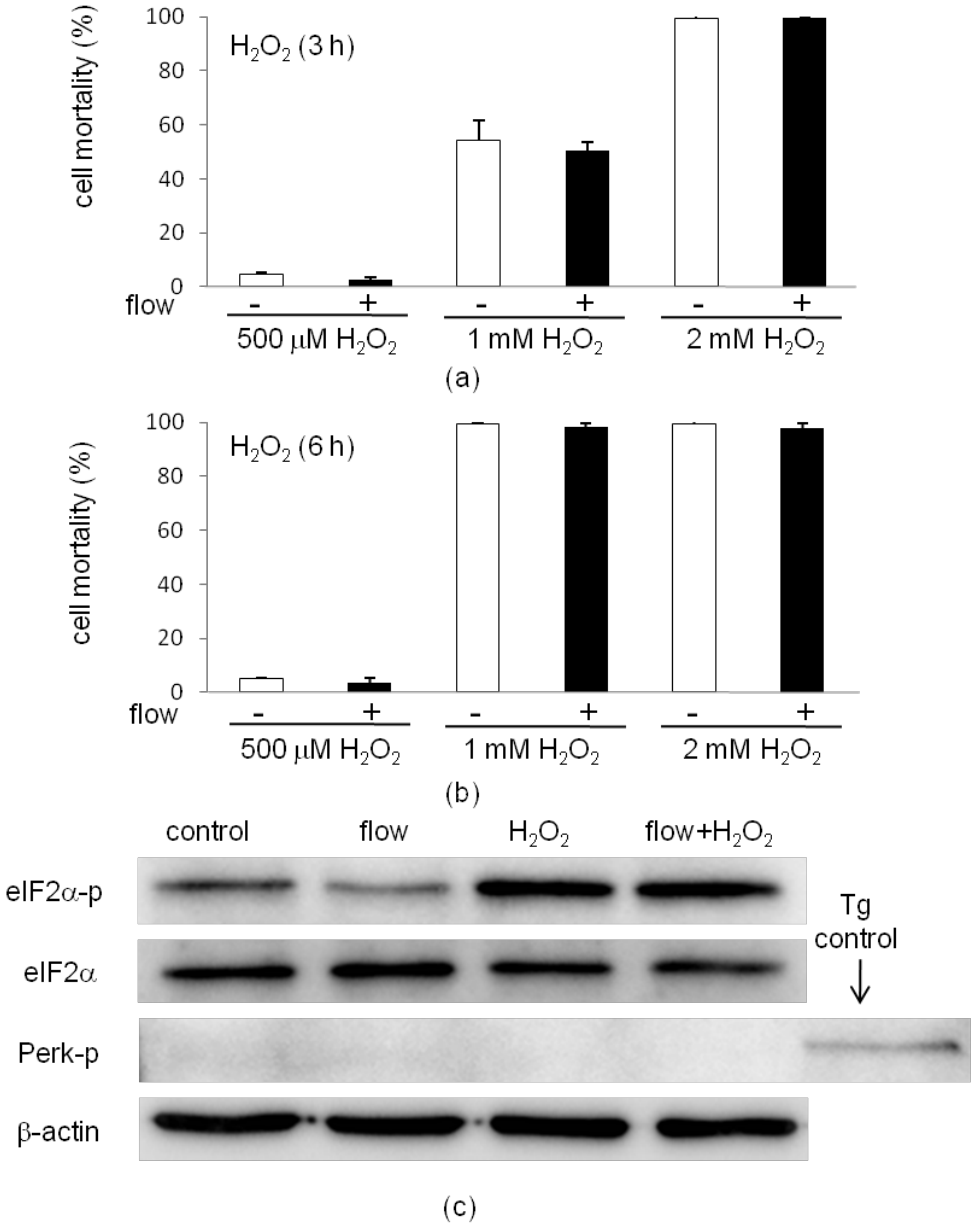

Figure 2.13 Responses to hydrogen peroxide in MC3T3 cells. (a) & (b) Cell mortality in response to 3 and 6 h incubation in the medium containing 0.5, 1 or 2 mM hydrogen peroxide, respectively. (c) Expression levels of eIF2α-p, eIF2α and Perk-p after 3 h incubation with 1mM H_2O_2

2.2.7 Effects of Perk siRNA on Tg-induced Cell Death

Since Tg activated phosphorylation of Perk and the flow pre-treatment partially inhibited its activation, we examined whether depleting Perk by siRNA would decrease Tg-driven cell mortality. Compared to normal control (no transfection), Perk siRNA reduced the Perk mRNA level to 14% (Figure 2.14 (a)). In agreement with the observed responses to stress to the ER, incubation with Tg for 8 h increased the cell mortality ratio to 17% (normal control) and 16% (siRNA control). Furthermore, 1 h flow pre-treatment reduced those mortality ratios down to 7% (normal control – white bars) and 5% (siRNA control – gray bars) (Figure 2.14 (b)). In the cells treated with Perk siRNA (black bars), no significant difference was observed in the cell mortality ratios between Tg alone and flow pre-treatment plus administration of Tg.

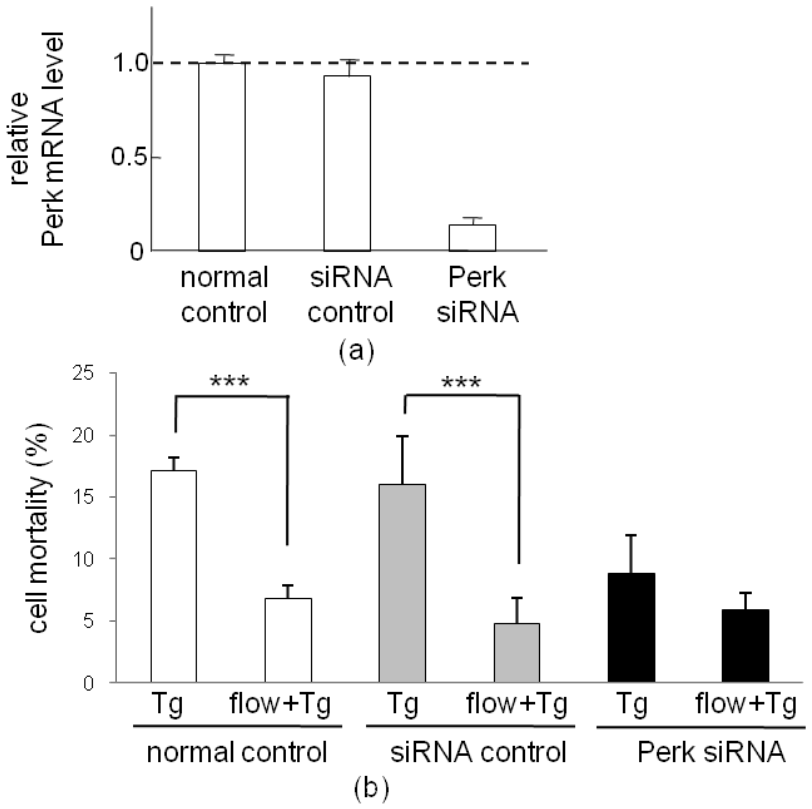

Figure 2.14 Effects of Perk siRNA on Tg-induced cell death. (a) Relative Perk mRNA levels in MC3T3 cells in normal control, siRNA control and Perk siRNA groups. (b) Cell mortality (in %) in response to 8 h incubation with Tg for normal control, siRNA control and Perk siRNA groups with and without 1 h flow pre-treatment

3. ECM-DEPENDENT VARIATIONS IN PHOSPHORYLATION PATTERNS OF GENES IN OSTEOBLAST-LIKE CELLS

In this chapter, molecular signaling involved in ECM geometry is presented. A genome-wide mRNA expression analysis was conducted using cells grown in the 2D and 3D models, and signaling pathways as well as active transcription factors were predicted. Real-time PCR, Western blot analysis and a mineralizing assay were conducted to verify the microarray-derived predictions.

3.1 Materials and Methods

3.1.1 Cell Culture

MC3T3 osteoblast-like cells (C4 clone) [12] were cultured in αMEM medium containing 10% FBS and antibiotics (50 units/ml penicillin and 50 µg/ml streptomycin; Invitrogen). Cells were incubated at 37ºC in a humid chamber with 5% CO_2 and prepared for experiments at 70 - 80% confluency. For the 2D model, approximately 4×10^5 cells were seeded in a 60 mm polystyrene tissue culture dish (Falcon), which was coated with rat-tail type I collagen (BD Bioscience). As a control, cells were also grown in the dish without coating type I collagen. For the 3D model, three concentrations (low density: 7×10^5 cells; medium density: 1.4×10^6 cells; and high density: 2.1×10^6 cells) of cells were seeded on the 3D collagen matrix (20 mm × 40 mm × 2 mm; CollaCote, Zimmer Dental), which was fabricated from bovine flexor tendon. To evaluate potential differences between the collagen solution used for the 2D model and the matrix form of collagen for

the 3D model, the collagen matrix was physically disrupted and the liquid form of collagen was extracted. These two sources of collagen were equally coated on the polystyrene dish, and the mRNA expression levels were compared. For evaluation of mRNA expression levels by real-time PCR and microarrays, cells were harvested 1 day after seeding. In evaluation of the role of p38 MAPK, cells were incubated in the presence of 10 μM SB203580 (Cat# 559398, Calbiochem).

3.1.2 Reverse Transcription and Real-time PCR

Using approximately 50 ng of total RNA, reverse transcription was conducted with high capacity cDNA reverse transcription kits (Applied Biosystems). Quantitative real-time PCR was performed using ABI 7500 with Power SYBR green PCR master mix kits (Applied Biosystems). We evaluated the mRNA levels of 5 osteogenic genes (Dentin matrix protein 1 – DMP1, Alkaline phosphatase – ALP, Bone sialoprotein – BSP, type I collagen – Col Iα1 and Osteocalcin – OCN), 3 transcriptional factors (Runx2, ATF4 and Osterix – Osx) [31-35], 2 cell cycle related genes (Cyclins E1 and E2) [36] and GAPDH. The PCR primers are listed in Table 3.1. The mRNA level of GAPDH was used as an internal control to calibrate potential variations in cell numbers in cell cultures. The relative mRNA levels of the selected genes were obtained with respect to the mRNA level of GAPDH for each sample, and relative mRNA abundance was determined as a ratio of the mRNA levels in the 3D model to those in the 2D model. The ratio of 1, for instance, implies that there is no difference in mRNA levels between the two models.

Table 3.1 Real-time PCR primers for the ECM geometry study

Gene	Forward primer	Backward primer
ALP	5’-CCGATGGCACACCTGCTT-3’	5’- GAGGCATACGCCATCACATG-3’
ATF4	5’-TGGCGAGTGTAAGGAGCTAGAAA -3’	5’- TCTTCCCCCTTGCCTTACG -3’
BSP	5’-ACCCCAAGCACAGACTTTTGA-3’	5’-CTTTCTGCATCTCCAGCCTTCT-3’
Col Iα1	5’- AAACTCCCTCCACCCCAATCT -3’	5’- TTTGGGTTGTTCGTCTGTTTCC -3’
Cyclin E1	5’-TGCCAAGATTGACAAGACTGTGA-3’	5’-TCCACGCATGCTGAATTATCA-3’
Cyclin E2	5’-GCCATCGACTCTTTAGAATTTCAATA-3’	5’-TCTTAACCACTTCAATGGAGGTAAAA-3’
DMP1	5’-GCGACGACCCCGAGAGTA-3’	5’-CTTTAGATTCTTCCGACCTGATACCA-3’
Osteocalcin	5’-CCGGGAGCAGTGTGAGCTTA-3’	5’-AGGCGGTCTTCAAGCCATACT-3’
Osterix	5’-CCCTTCTCAAGCACCAATGG -3’	5’-AGGGTGGGTAGTCATTTGCATAG-3’
Runx2	5’- AAATGCCTCCGCTGTTATGAA -3’	5’- GCTCCGGCCCACAAATCT -3’
GAPDH	5’- TGCACCACCAACTGCTTAG -3’	5’- GGATGCAGGGATGATGTTC -3’

3.1.3 Microarray Analysis

Microarray experiments were conducted using Agilent whole mouse genome arrays (G4112A, Agilent). A total of 8 RNA samples were isolated with an RNeasy Plus mini kit (Qiagen) from 4 pairs of cells grown in the 2D and 3D substrates for 24 h. They were labeled with Agilent low RNA input fluorescent linear amplification kits and hybridized to 8 one-color arrays using in situ hybridization kits (Agilent).

Data were filtered to remove background noise, and a modified t-test was performed to identify a group of genes that were altered > 2-fold or < 0.5-fold with statistical significance at $p < 0.01$. The list of genes identified was imported into Pathway-Express, which was used to predict molecular signaling pathways through evaluation of an impact factor that accounts for contributions of the proportion of differentially regulated genes on the pathway [37-38].

MotifModeler II was employed to predict transcription factors involved in the microarray derived data [39]. The raw data generated from the 8 arrays were imported into the Partek Software and signal intensity for each probe set was evaluated. Quantile normalization was then performed and the normalized signals were further adjusted by aligning medium values [40]. The probe sets whose expression levels were below a threshold in each condition were then removed. Differentially expressed genes in the 2D and 3D conditions were then selected using Student t-test.

3.1.4 Western Blot Analysis

To evaluate the role of kinases linked to the predicted signaling pathways, we conducted Western blot analysis. Cells were sonicated using a sonic dismembrator (Model 100, Fisher Scientific) and lysed in a RIPA lysis buffer containing protease inhibitors (Santa Cruz Biotech) and phosphatase inhibitors (Calbiochem). Isolated proteins were fractionated using 10% SDS gels and electro-transferred to Immobilon-P membranes (Millipore). The membrane was incubated for 1 h with primary antibodies

followed by 45 min incubation with goat anti-rabbit IgG (Cell Signaling Tech) or goat anti-mouse IgG conjugated horseradish peroxidase (Amersham Biosciences). We used antibodies against ERK1/2, p-ERK1/2 (Thr202/Tyr204), p38MAPK, p-p38MAPK (Thr180/Tyr182), p-p130Cas (Tyr410) (Cell Signaling Tech), p-FAK (Tyr861) (Santa Cruz Biotech) and β-actin (Sigma). Protein levels were assayed using an ECL advance Western blotting detection kit (Amersham Biosciences), and signal intensities were quantified with a luminescent image analyzer (LAS-3000, Fuji Film).

3.1.5 Mineralization Assay

Mineralization of ECM was assayed by Alizarin red S staining [41]. Prior to culturing cells in mineralizing medium, approximately 1×10^6 cells were grown in the αMEM medium for 2 days. Then, 50 μg/ml of ascorbic acid (Sigma) was added (day 1), and 5 mM β-glycerophosphate (Sigma) was added on the next day (day 2). The medium was changed every 2 or 3 days, and staining was conducted on day 8. The earlier staining on day 8 rather than day 10 or later was chosen to evaluate accelerated differentiation in the 3D model. Cells were washed with PBS three times and fixed with ice-cold 70% ethanol for 1 h followed by several washes with distilled water. They were stained with 2% Alizarin red S (pH 4.2) (Sigma) for 10 min and washed with distilled water.

3.1.6 Statistical Analysis

Experiments were conducted twice (Western blotting) and four times (PCR), and the data were expressed as mean ± s.d. Statistical significance from a t-test was evaluated at $p < 0.05$.

Regarding the prediction of transcription factors that potentially caused differential expression patterns in the 2D and 3D models, 382 differentially expressed genes were selected from the microarray data. These genes presented alterations of their mRNA expression levels (> 2-fold or < 0.5-fold) with statistical significance at $p < 0.01$.

Among them, 367 genes were used for the prediction with MotifModeler II, since 15 genes in the microarray data did not have their Entrez ID. MotifModeler II provides two scores for each of the potential transcription factors: the TCS score is calculated by how well its occurrences in the promoter or 3'-UTR correlate with the expression level difference, in the context of combinatorial regulation, and the Xm score evaluates its potential function on the global gene expression. A positive and negative Xm imply that its occurrence in the gene regulatory region contributes to the global gene over and under-expression in the 3D samples compared with the 2D samples [39].

3.2 Results

3.2.1 Altered Messenger RNA Expression on Day 1 between 2D and 3D Substrates

We first examined alterations in mRNA expression on day 1. Compared to the cells in the 2D model, relative mRNA abundance of three genes (DMP1, BSP and OCN) was significantly elevated in the 3D model (Figure 3.1 (a)). For instance, DMP1 abundance was 5.2 times higher in the 3D model (low cell density culture) than in the 2D model. Interestingly, the OCN mRNA level was elevated 18.5 times in the 3D model, while relative mRNA abundance of Collagen Iα1 was unchanged.

We next evaluated relative mRNA abundance of transcription factors (Runx2, ATF4 and Osx). The relative mRNA levels of Runx2 and ATF4 did not change either at 2 h or 24 h, while the relative level of Osx mRNA at 2 h after seeding was higher in the 3D model than that in the 2D model (Figure 3.1 (b)). Furthermore, the density of cells in the 3D culture did not significantly affect the relative mRNA expression levels (data not shown).

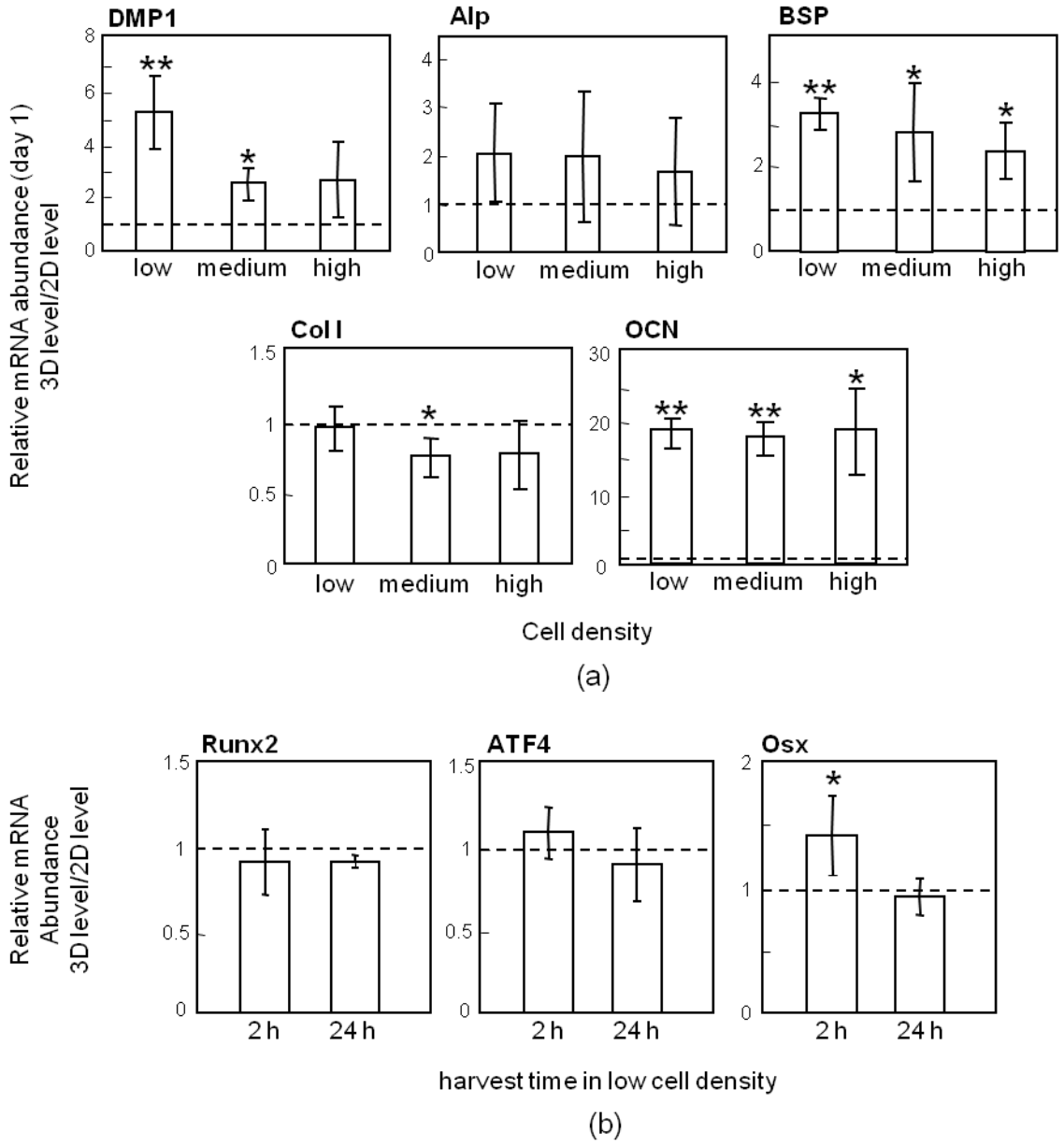

Figure 3.1 Relative mRNA abundance in the 3D model. The relative mRNA expression level in the 3D model was normalized by the level in the 2D model. The asterisks indicate statistical significance at $p < 0.05$ (*) and $p < 0.01$ (**), and the dotted line shows the normalized ratio of 1. (a) Relative mRNA abundance of 5 anabolic genes (DMP1, ALP, BSP, Col Iα1 and OCN) at 24 h. (b) Relative mRNA abundance of 3 transcriptional factors (Runx2, ATF4 and Osx) at 2 and 24 h

3.2.2 Effect of Collagens in 2D and 3D Substrates

For three genes (DMP1, BSP and OCN) whose mRNA levels were elevated in the 3D model, we examined their expression levels in the 2D model with and without collagen coating (Figure 3.2).

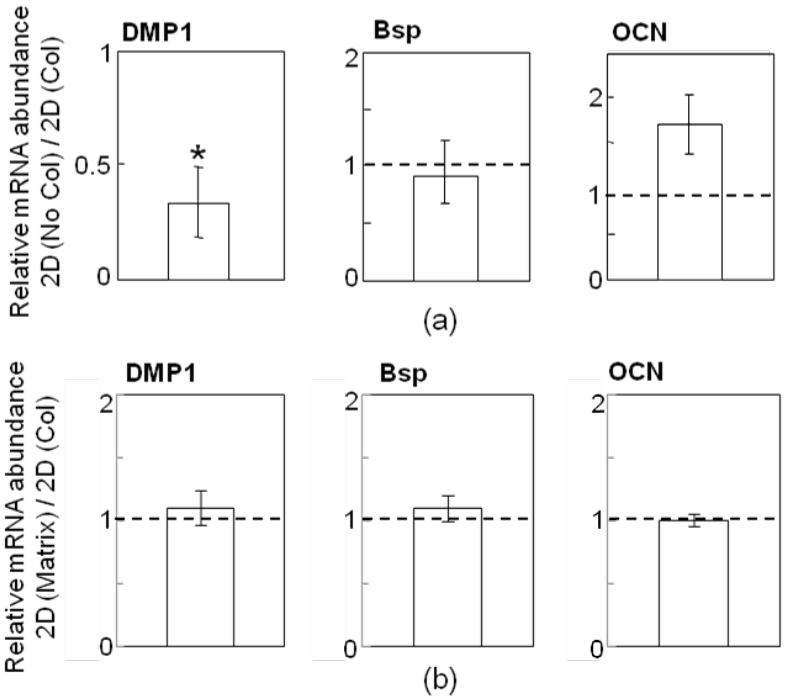

Figure 3.2 Effects of collagen coating. The relative mRNA levels of DMP1, BSP and OCN in the 2D model with and without collagen coating. The asterisk indicates statistical significance at $p < 0.05$, and the dotted line shows the normalized ratio of 1. Note that 2D (No Col) = no collagen coating, 2D (Col) = coating with liquid collagen, and 2D (Matrix) = coating with collagen extracted from 3D matrix. (a) Comparison between 2D (No Col) and 2D (Col). (b) Comparison between 2D (Matrix) and 2D (Col)

Compared to the substrate coated with type I collagen, the DMP1 mRNA levels were reduced on the polystyrene surface without collagen coating. The levels of BSP and OCN mRNAs were not, however, significantly altered (Figure 3.2 (a)). We further examined any differential effect between two collagen sources (liquid collagen in the 2D model and the collagen extracted from the 3D matrix). Between these two forms of collagen coating on the culture dishes, where 2D (Matrix) = coating with collagen extracted from 3D matrix and 2D (Col) = coating with liquid collagen, no significant

expressional differences were observed in the relative mRNA abundance in DMP1, BSP and OCN.

3.2.3 Suppression of Focal Adhesion Pathways in the 3D Culture

To identify potential molecular pathways that promote mineralization in the 3D model, microarray experiments and Pathway-Express software were employed. Focal adhesion pathway was selected, in which, 39 genes out of 60 were down-regulated in the 3D model (Figure 3.3). This pathway included 8 regulatory subunits: ECM-receptor interaction, cytokine-cytokine receptor interaction, phosphatidyl inositol signaling system, regulation of actin cytoskeleton, Wnt signaling pathway, apoptosis, MAPK signaling pathway and cell cycle.

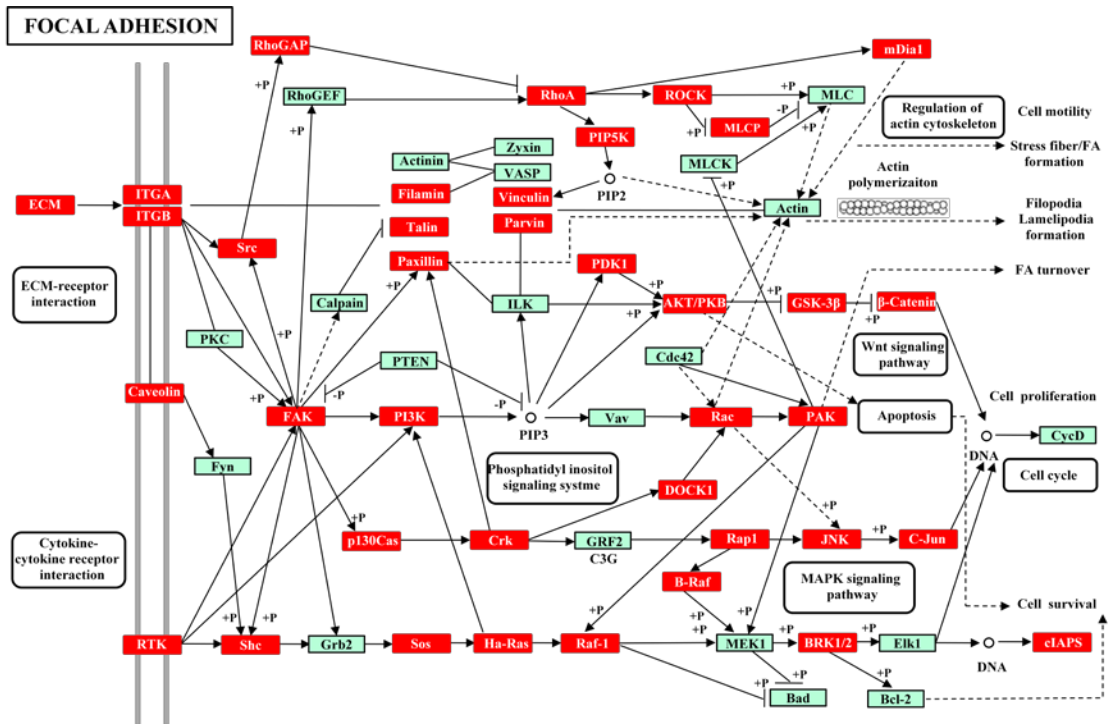

Figure 3.3 Focal adhesion pathways. Molecular network in the focal adhesion pathway. Note that 39 out of 60 genes were down-regulated in the 3D model (shown in red). The pathway includes 8 regulatory subunits such as ECM-receptor interaction, cytokine-cytokine receptor interaction, phosphatidyl inositol signaling system, regulation of actin cytoskeleton, Wnt signaling pathway, apoptosis, MAPK signaling pathway and cell cycle

Since phosphorylated ERK1/2 can stimulate cell proliferation as well as cell cycling, we assayed the phosphorylation level of ERK1/2. At both 30 min and 60 min after cell seeding, the level of its phosphorylated form (p-ERK1/2) was reduced more in the 3D model than in the 2D model (Figure 3.4 (a)). The results were consistent with the notion that the 3D environment has a suppressive effect on the proliferation of osteoblasts.

In order to verify involvement of a docking protein as well as a key kinase in focal adhesion, we evaluated the phosphorylated levels of p130Cas (p-p130Cas, tyr410) and FAK (p-FAK, tyr861). Those phosphorylation sites are known to be important for stimulating cell adhesion [42]. The results revealed that their phosphorylated levels were attenuated in the 3D model (Figure 3.4 (b)).

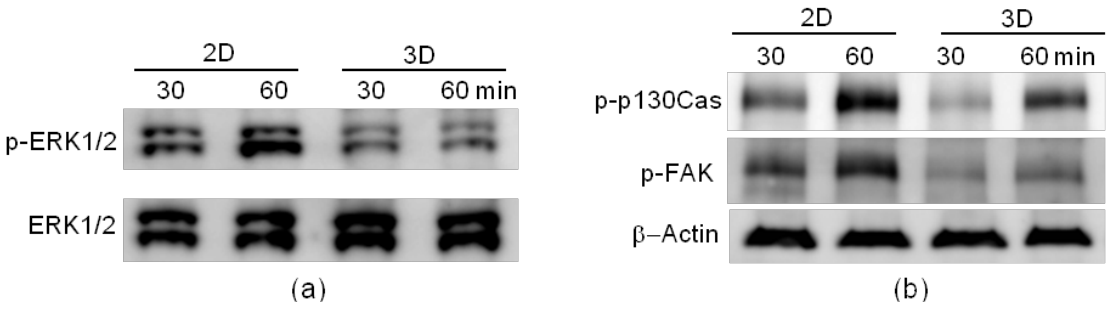

Figure 3.4 Comparison of the expression levels of phosphorylated forms of ERK1/2, p130Cas and FAK in 2D and 3D model. (a) Down-regulated p-ERK1/2 in the 3D model at 30 and 60 min (b) Decrease in the phosphorylated levels of p130Cas (tyr 410) and FAK (tyr861) in the 3D model at 30 and 60 min

3.2.4 Suppression of Cell-cycle Related Genes in the 3D Culture

The cell-cycle pathway was selected as well according to the results from Pathway-Express. Four regulatory subunits were included in this pathway: MAPK signaling pathway, apoptosis, DNA biosynthesis and ubiquitin mediated proteolysis. Note that the subunits linked to cell cycle, MAPK signaling pathway and apoptosis were also included in the cell adhesion pathway.

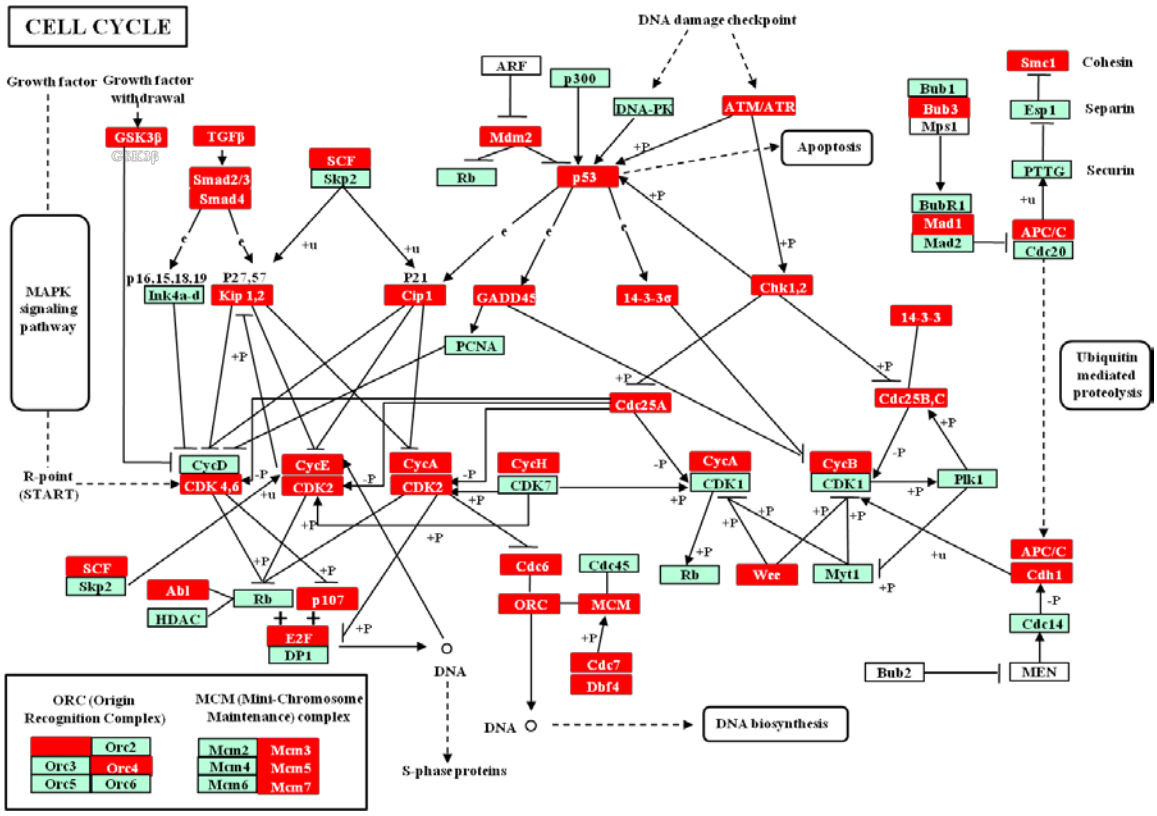

Figure 3.5 Cell-cycle pathways. Molecular network in the cell-cycle pathway. Note that 38 out of 64 genes were down-regulated in the 3D model (shown in red). The pathway includes 4 regulatory subunits such as MAPK signaling pathway, apoptosis, DNA biosynthesis and ubiquitin mediated proteolysis

In order to verify array-derived expression data, we conducted real-time PCR and confirmed the mRNA levels of Cyclins E1 and E2. It has been shown that these cyclins bind to CDK2 and promote the transition from G1 to S phase [37]. Our PCR results were consistent with the pathway prediction, showing that the relative mRNA levels of those two cyclin genes were reduced in the 3D model. Compared to the low density culture, the high density culture exhibited a stronger decrease in the mRNA level of those two Cyclin genes (Figure 3.6).

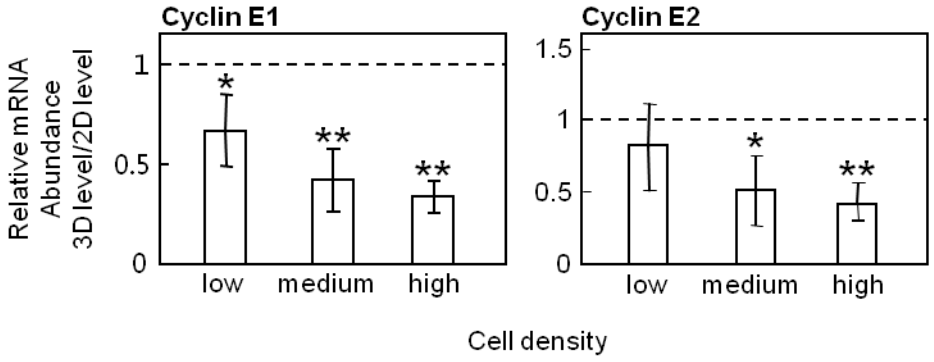

Figure 3.6 Suppression of relative mRNA abundance of Cyclins E1 and E2 in the 3D model. The dotted line shows the normalized ratio of 1

3.2.5 Transcription Factor Prediction

Table 3.2 lists the predicted transcription factors whose TCS scores are larger than a threshold value defined as (mean value + 3 × standard deviation). Among 7 transcription factors, the positive Xm score (stimulatory in the 3D model) was given to NF-κB and the negative Xm (inhibitory in the 3D model) to AIRE (autoimmune regulator), AP-4 (activating enhancer binding protein 1), STAT (signal transducers and activator of transcription) and HEB (HeLa E-box binding protein).

Table 3.2 Predicted transcription-factor binding motifs

Accession	Transcription Factors	TCS score	Xm Score
M00999	AIRE	2.69e-03	-1.14e+06
M00927	AP-4	2.68e-03	-1.35e+06
M00279	MIF-1	2.68e-03	-1.33e+06
M00070	Tal-1beta:ITF-2	2.67e-03	-1.17e+06
M00051	NF-kappaB (p50)	2.66e-03	9.98e+05
M00223	STATx	2.65e-03	-1.28e+06
M00698	HEB	2.65e-03	-1.33e+06

3.2.6 Involvement of p38 MAPK in Expression of DMP1 and BSP

Two of the osteogenic genes (DMP1 and BSP) exhibited significantly elevated mRNA expression levels on days 1 and 8. It has been reported that expression of DMP1 is activated by p38 MAPK [24], which is part of the predicted cell cycle pathway.

Western blots showed that the level of phosphorylated p38 MAPK was higher in the 3D model than in the 2D model (Figure 3.7 (a)). In order to examine the role of p38 MAPK in expression of DMP1 and BSP, we employed a p38 MAPK inhibitor (SB203580). The result demonstrated that this pharmacological agent suppressed relative mRNA abundance of DMP1 and BSP (Figure 3.7 (b)). In the 3D model, a normalized induction ratio (based on expression in 2D without SB203580) changed from 9.7 ± 1.3 (mean ± s.d.) to 4.8 ± 1.6 (DMP1) and from 2.0 ± 0.8 to 0.61 ± 0.15 (BSP).

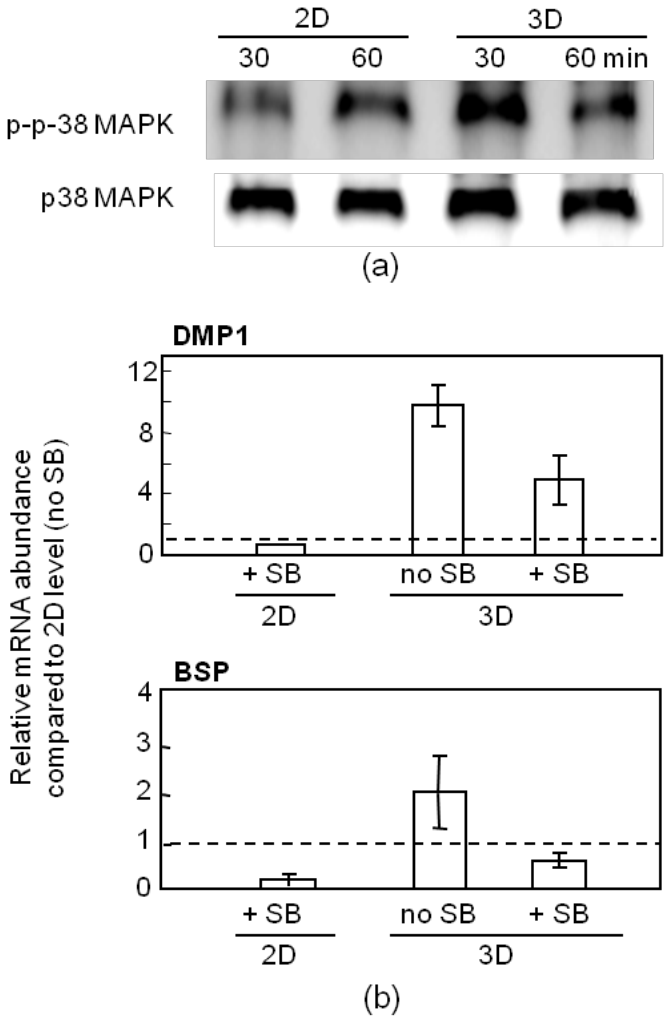

Figure 3.7 Linkage of phosphorylation of p38 MAPK to relative mRNA abundance of DMP1 and BSP. (a) Activation of p-p38 MAPK in the 3D model. (b) Suppression of relative mRNA abundance of DMP1 and BSP by 10 μM SB203580 in the 2D and 3D models. The dotted line shows the normalized ratio of 1

3.2.7 Enhanced Mineralization on Day 8 in 3D Environment

In the presence of ascorbic acid the degree of mineralization was assayed 8 days after addition of β-glycerophosphate with Alizarin red S. This dye produces red staining for crystallized calcium salts [31]. The level of red staining intensity was increased in cells grown in the 3D matrix (Figure 3.8), indicating that the 3D environment stimulates differentiation of osteoblasts.

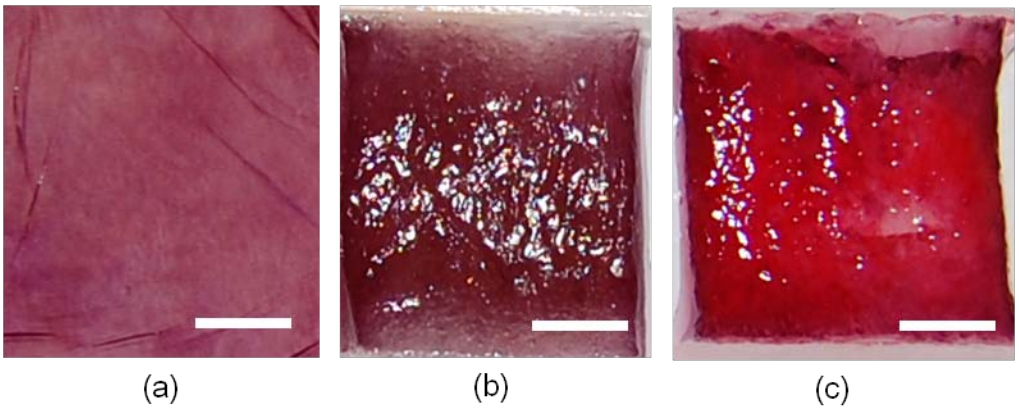

Figure 3.8 Alizarin staining for the 2D and 3D models. (a) Alizarin staining for the 2D model. (b) Alizarin staining for the 3D control matrix (no cells). (c) Alizarin staining for the 3D model. White bar = 5 mm

The results with real-time PCR revealed that compared to cells in the 2D model, relative mRNA abundance of DMP1 (6.77 ± 1.44; mean ± s.d.), ALP (2.82 ± 0.16), and BSP (1.19 ± 0.06) was significantly up-regulated in the 3D model (Figure 3.9), although the OCN mRNA level (0.68 ± 0.06) was down-regulated.

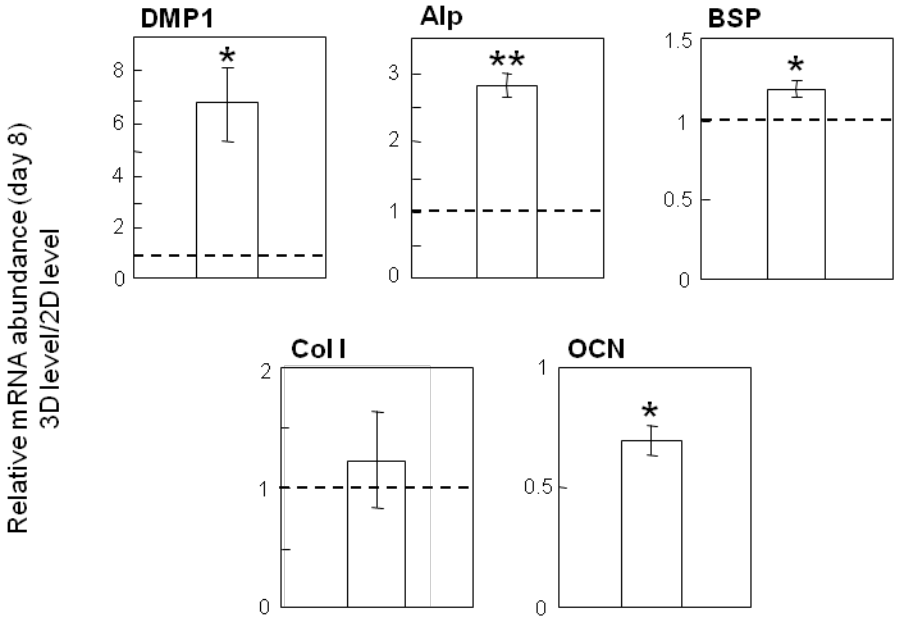

Figure 3.9 Ascorbic-acid stimulated mineralization and mRNA up-regulation of the select osteogenic genes in the 3D model on day 8. Relative mRNA abundance of DMP1, ALP, BSP, Col Iα1 and OCN as a ratio of expression in the 3D model to that in the 2D model. The dotted line (normalized ratio of 1) indicates no change in mRNA levels in the 2D and 3D models. The asterisks indicate statistical significance at $p < 0.05$ (*) and $p < 0.01$ (**), and the dotted line shows the normalized ratio of 1

4. DISCUSSION

The present studies demonstrated signaling pathways involved in mechanical stimulation and ECM geometry in osteoblasts. The mechanical stimulation study focused on eIF2α-mediated responses, while the ECM geometry study focused on genome-wide pathway analysis.

4.1 Discussion on the Mechanical Stimulation Study

In the first study, the results showed that mechanical stimulation reduced the levels of Perk-p and eIF2α-p, and suppressed cell death caused by Tg-induced stress to the ER. Western analysis showed that the active phosphorylated form of Perk, induced by Tg and Tn, was down-regulated by mechanical stimulation although the load-driven expression profile of ATF4 in Figure 2.9 was not identical in response to Tg and Tn. Since depleting the expression of Perk by siRNA in Tg-treated cells reduced the cell mortality ratio regardless of application of fluid shear, we postulated that Perk was involved in the interplay of mechanical stimulation and Perk-mediated cellular stress (Figure 4.1). Note that fluid shear did not suppress cell death induced by H_2O_2, since H_2O_2 driven elevation of the level of eIF2α-p was not mediated by Perk.

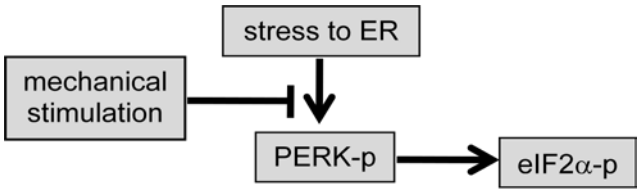

Figure 4.1 Schematic diagram illustrating the effects of ER stress and mechanical stimulation on Perk-p and eIF2α-p

Our molecular analysis indicated the complex interactions at the transcriptional and translational levels between ER mediated stress and mechanical stimulation. The genes directly responsive to stress to the ER, such as Xbp1, ATF6 and CHOP, were up-regulated by Tg and partially suppressed by mechanical stimulation. It is reported that in the ER membrane of stressed cells, IRE1 can remove a 26-nucleotide intron from unspliced Xbp1 mRNA by its RNase activity. Then the two ends of the mRNA are ligated, resulting in a frame shift in the coding sequence. The spliced Xbp1 mRNA encodes a potent transcriptional activator of many genes involved in unfolded protein responses (UPR) [43-44]. In the current study, Xbp1 was actively spliced by Tg, and this splicing event was suppressed by mechanical stimulation. ATF6 is activated by Tg and induces gene expression to alleviate stress to ER [45]. Due to the role of CHOP in an apoptotic pathway [46] through activation of Perk [47], the load-driven suppression of CHOP was consistent with the observed reduction in cell mortality. In addition, mRNA levels of ATF3 [48] and ATF4 [49] were increased by Tg regardless of mechanical stimulation. Note that CHOP can also be up-regulated through activation of ATF4, ATF6 and Xbp1 [50].

Protein expression analysis supported the role of mechanical stimulation in stress-linked translational regulation. In concert with the observed suppression of cell death, mechanical stimulation down-regulated the protein levels of eIF2α-p and CHOP. Although the basal expression level of Perk protein was undetectably low, the elevated level of Perk-p in Tg treated cells was decreased by flow pre-treatment. Furthermore, Tg driven cell death was mediated by Perk-p and the reduction in Perk-p by mechanical stimulation decreased cell mortality. Besides, the Perk siRNA treated group showed the reduced level of cell mortality, suggesting the correlation between the expression level of Perk and cell death. In addition, the fact that flow pre-treatment did not significantly modulate the cell mortality in the Perk siRNA treated group also supports the correlation between the expression level of Perk and mechanical loading. Therefore mechanical stimulation and cell mortality were connected through Perk. It is well known that mechanical stimulation enhances bone formation [6-8]. Thus, it is conceivable that

reduction of cell death through regulation of Perk and eIF2α may enhance cellular survival and contribute to bone formation. Note that Perk knockout mice die with severe diabetic and skeletal defects [51], thus Perk has an indispensible role in the development of bone.

Suppression of cell death by mechanical stimulation is considered to be mediated by multiple signaling pathways. Besides the Perk and eIF2α effects identified in this study, it has been shown that apoptosis of osteoblasts caused by TNFα and serum deprivation are suppressed by mechanical stimulation through a PI3K pathway [9] and a Wnt signaling pathway [52], respectively. In accordance with those observations, our previous *in vivo* data revealed that mechanical loading activated both PI3K and Wnt pathways [53]. Taken together, load-driven suppression of cell mortality is mediated through multiple signaling pathways including the eIF2α pathway as well as the PI3K and Wnt signaling pathways. Since cytoplasmic concentration of calcium ions is altered by stress to the ER as well as mechanical stimulation, the regulation of calcium ions might be involved in the observed alteration in Perk phosphorylation.

4.2 Discussion on the ECM Geometry Study

In the second study, two molecular signaling pathways – focal adhesion and cell cycling – were predicted as the potential modulators of the proliferation and differentiation of osteoblasts in the two ECM environments using genome-wide analysis. Transcription factors as well as the binding sites relating with ECM geometry variations were predicted. Associated with enhanced mineralization in the 3D culture, relative mRNA abundance of the selected osteogenic genes such as DMP1 and BSP were elevated in the 3D model. The proteome analysis for phosphorylation verified that in accordance with the diminished role of focal adhesion and cell cycling in the 3D model, the levels of p-p130Cas, p-FAK and p-ERK1/2 were decreased. Phosphorylation of FAK at tyr861 is known to induce interaction with p130Cas. The level of p-p38 MAPK was elevated in cells seeded in the 3D model, and inhibition of p-p38 MAPK by 10 μM of

SB203580 reduced relative mRNA abundance of DMP1 and BSP. Consequently, the present study supports the notion that differential gene expression and altered osteoblastic fates in the 2D and 3D models are linked to focal adhesion and cell cycling through modulations in the phosphorylation pattern of kinases and a docking protein.

By analyzing microarray data, we also predicted the most influential transcription factors that potentially cause the differences in global gene expression profile between 2D and 3D models. In the 6 transcription factors that were predicted to contribute to the gene under expression in 3D samples, SATA was reported to promote osteoblast differentiation [54]. As to the transcription factor that was predicted to contribute to gene over expression in 3D samples in comparison with 2D samples, inactivation of NF-κB was reported to be involved with osteoblast development [55]. One potential interpretation is that, decreased level of SATA was contributing to under expression of genes involving in osteoblast differentiation in 3D sample, while decreased expression level of NF-κB was contributing to the over expression of genes involved in osteoblast development in 3D samples.

The observed reduction in proliferation and enhancement of mineralization in the 3D model is consistent with previous reports in which bone marrow-derived cells [56] or adult human osteoblasts [17] grown in native collagen gels stopped proliferation and exhibited higher alkaline phosphatase activity. However, those cells grown in a solidified collagen gel had restricted medium circulation as well as a limited migration space. In our 3D model, cells were seeded on a porous type I collagen matrix whose typical pore size ranged from 10 to 100 μm. Thus, the retarded proliferation in our 3D model is less influenced by physical or chemical confinement than the previous studies. Our results show that osteoblasts in the 3D environment promote differentiation by suppressing the cell adhesion and cell cycle pathways. Note that since the mRNA levels of Cyclins E1 and E2 were down-regulated the most in the 3D culture with the highest number of cells, cell density is also a factor to regulate cellular proliferation. However, up-regulation of the selected osteogenic genes was largely insensitive to cell density.

In a focal adhesion pathway, FAK serves as a marker for focal adhesions as a non-receptor focal adhesion kinase. Consistent with its reduced phosphorylation level in the 3D model, down-regulation of its auto-phosphorylation is reported in vascular smooth muscle cells in a honeycomb-like mesh substrate [57]. Interestingly, we observed in the 3D environment that the level of p-ERK1/2 was suppressed, while that of p-p38 MAPK was elevated and its up-regulation was linked to mRNA up-regulation of DMP1 and BSP. In response to mechanical stimulation, osteoblasts are known to activate FAK and increase the level of p-ERK1/2 [58]. Thus, it is conceivable that the 3D environment would offer a stimulus that would act oppositely to mechanical stimulation. However, there is a report that fluid flow to mesenchymal stem cells cultured in a bone-like ECM matrix stimulates osteoblastic differentiation [59].

Although most of the selected osteogenic genes were up-regulated in the 3D model, we observed their differential temporal responses. For instance, expression of DMP1 and BSP was up-regulated on both day 1 and day 8. Expression of OCN was, however, elevated on day 1 and decreased on day 8. Furthermore, in spite of ~ 20 times increase in relative OCN mRNA abundance in the 3D model on day 1, relative mRNA abundance of Runx2 or ATF4 was unchanged. The results indicate a possibility that post-transcriptional regulation of Runx2 or ATF4 is needed to activate OCN transcription [34]. The observed up-regulation of Osx expression in the 3D model is agreeable with the understanding that osteoblast differentiation is mediated by p38 MAPK through Osx [60].

4.3 Limitations and Future Direction

There are several limitations in the present study. First, in the mechanical stimulation study, the relationship of shear stress and mRNA expression levels of stress response genes needs to be further confirmed and studied. Second, further evidence needs to be provided to support the causal relationship between mechanical stimulation and the reduced level of Perk phosphorylation. Third, in the ECM geometry study, the ECM differences between the 2D and 3D models here not only include geometric configuration

but also variations in cell density, collagen structures and mechanical properties. Although we employed three cell densities and two collagen sources for 2D models, the two signaling pathways examined herein are potentially affected not only by 2D/3D differences but also by other causes including differences in mechanical properties of the cells in culture. Fourth, we investigated the initial response (up to 1 h) for phosphorylation patterns, the 1-day response for genome-wide mRNA levels, and the 8-day outcome for mineralization. However, the signaling pathways were temporarily regulated, and other molecular networks can be involved in different time periods. Lastly, the ECM geometry study was based on a single cell line, and further verification is necessary using primary cells.

The two studies in the thesis are both bone cell signaling pathway studies. As we know, bone diseases, like osteoporosis and oestopenia, can reduce bone mass and strength and increase the possibility of fracture or bone necrosis, which can significantly affect quality of life. Studies have found that some bone diseases are directly or indirectly related with stress to ER. Our mechanical study potentially provides a therapeutic treatment by focusing on phosphorylation of eIF2α which is a response to ER stress. In the ECM geometry study, we have found that the 3D culture environment employed in the current study stimulated differentiation of osteoblasts through suppression of the cell adhesion and cell cycling pathways, and we have also shown that the 3D model reduces the levels of p-130Cas, p-FAK and p-ERK1/2 while elevating that of p-p38 MAPK. The results would be useful in developing an *in vitro* assay for regulating proliferation and differentiation of bone forming cells.

In the future, the mechanical stimulation study can be further developed by studying behavior differences of young osteoblasts and aged osteoblasts in response to mechanical stimulation. The ECM geometry study can also be extended to primary bone cells, e.g. MSCs. Also, the role of the predicted transcription factors should be further evaluated in the 2D and 3D models.

5. CONCLUSION

Signaling pathways involved in mechanical stimulation and ECM geometry in bone cells were studied to examine the role of cellular stress to osteoblastic fates. Specifically, eIF2α pathways in response to mechanical stimulation in Aim 1 and phosphorylation patterns of p130Cas, FAK, ERK and p38MAPK in response to ECM variations in Aim 2 were analyzed.

In the eIF2α pathway study in Aim 1, two flow systems were developed to induce mechanical loading to bone cells. A joint loading method was developed to apply mechanical loading to mouse ulnae. According to both *in vitro* and *in vivo* experimental results, it was concluded that load-driven suppression of cell mortality is achieved through multiple signaling pathways, including the Perk mediated eIF2α pathway, and this study supports the notion that mechanical stimulation is a suppressor of Perk-mediated stress and cell death. In the ECM geometry study in Aim 2, a 3D culture environment was employed to stimulate differentiation of osteoblasts through suppression of the cell adhesion and cell cycling pathways. The 3D model was shown to reduce the levels of p-130Cas, p-FAK and p-ERK1/2 while elevating that of p-p38 MAPK.

In summary, the present studies will be useful in establishing *in vitro* assay for regulating proliferation and differentiation of bone forming cells and identifying new therapeutic targets for bone diseases.

LIST OF REFERENCES

LIST OF REFERENCES

[1] R. J. Kaufman, "Stress signaling from the lumen of the endoplasmic reticulum: coordination of gene transcriptional and translational controls," *Genes Dev,* vol. 13, pp. 1211-33, May 1999.

[2] H. P. Harding, *et al.*, "An integrated stress response regulates amino acid metabolism and resistance to oxidative stress," *Mol Cell,* vol. 11, pp. 619-33, Mar 2003.

[3] C. G. Proud, "eIF2 and the control of cell physiology," *Semin Cell Dev Biol,* vol. 16, pp. 3-12, Feb 2005.

[4] R. C. Wek, *et al.*, "Coping with stress: eIF2 kinases and translational control," *Biochem Soc Trans,* vol. 34, pp. 7-11, Feb 2006.

[5] C. Xu, *et al.*, "Endoplasmic reticulum stress: cell life and death decisions," *J Clin Invest,* vol. 115, pp. 2656-64, Oct 2005.

[6] T. M. Skerry and L. J. Suva, "Investigation of the regulation of bone mass by mechanical loading: from quantitative cytochemistry to gene array," *Cell Biochem Funct,* vol. 21, pp. 223-9, Sep 2003.

[7] P. Zhang, *et al.*, "Knee loading stimulates cortical bone formation in murine femurs," *BMC Musculoskelet Disord,* vol. 7, p. 73, Sep 2006.

[8] M. Grellier, *et al.*, "Responsiveness of human bone marrow stromal cells to shear stress," *J Tissue Eng Regen Med,* vol. 3, pp. 302-9, Jun 2009.

[9] F. M. Pavalko, *et al.*, "Fluid shear stress inhibits TNF-alpha-induced apoptosis in osteoblasts: a role for fluid shear stress-induced activation of PI3-kinase and inhibition of caspase-3," *J Cell Physiol,* vol. 194, pp. 194-205, Feb 2003.

[10] D. J. Hadjidakis and Androulakis, II, "Bone remodeling," *Ann N Y Acad Sci,* vol. 1092, pp. 385-96, Dec 2006.

[11] I. Kalajzic, *et al.*, "Dentin matrix protein 1 expression during osteoblastic differentiation, generation of an osteocyte GFP-transgene," *Bone,* vol. 35, pp. 74-82, Jul 2004.

[12] G. Xiao, *et al.*, "Ascorbic acid-dependent activation of the osteocalcin promoter in MC3T3-E1 preosteoblasts: requirement for collagen matrix synthesis and the presence of an intact OSE2 sequence," *Mol Endocrinol,* vol. 11, pp. 1103-13, Jul 1997.

[13] R. L. Jilka, "Molecular and cellular mechanisms of the anabolic effect of intermittent PTH," *Bone,* vol. 40, pp. 1434-46, Jun 2007.

[14] J. Rubin, *et al.*, "Molecular pathways mediating mechanical signaling in bone," *Gene,* vol. 367, pp. 1-16, Feb 2006.

[15] K. Hamamura and H. Yokota, "Stress to endoplasmic reticulum of mouse osteoblasts induces apoptosis and transcriptional activation for bone remodeling," *FEBS Lett,* vol. 581, pp. 1769-74, May 2007.

[16] J. Wei, *et al.*, "PERK is essential for neonatal skeletal development to regulate osteoblast proliferation and differentiation," *J Cell Physiol,* vol. 217, pp. 693-707, Dec 2008.

[17] A. Rattner, *et al.*, "Mineralization and alkaline phosphatase activity in collagen lattices populated by human osteoblasts," *Calcif Tissue Int,* vol. 66, pp. 35-42, Jan 2000.

[18] H. Yokota and S. M. Tanaka, "Osteogenic potentials with joint-loading modality," *J Bone Miner Metab,* vol. 23, pp. 302-8, Jul 2005.

[19] S. B. Cullinan and J. A. Diehl, "Coordination of ER and oxidative stress signaling: the PERK/Nrf2 signaling pathway," *Int J Biochem Cell Biol,* vol. 38, pp. 317-32, Mar 2006.

[20] A. A. Fatokun, *et al.*, "Responses of differentiated MC3T3-E1 osteoblast-like cells to reactive oxygen species," *Eur J Pharmacol,* vol. 587, pp. 35-41, Jun 2008.

[21] K. Hamamura, *et al.*, "Ganglioside GD3 promotes cell growth and invasion through p130Cas and paxillin in malignant melanoma cells," *Proc Natl Acad Sci U S A,* vol. 102, pp. 11041-6, Aug 2005.

[22] K. Hamamura, *et al.*, "Focal adhesion kinase as well as p130Cas and paxillin is crucially involved in the enhanced malignant properties under expression of ganglioside GD3 in melanoma cells," *Biochim Biophys Acta*, vol. 1780, pp. 513-9, Mar 2008.

[23] S. Kapur, *et al.*, "Extracellular signal-regulated kinase-1 and -2 are both essential for the shear stress-induced human osteoblast proliferation," *Bone*, vol. 35, pp. 525-34, Aug 2004.

[24] K. Narayanan, *et al.*, "Transcriptional regulation of dentin matrix protein 1 by JunB and p300 during osteoblast differentiation," *J Biol Chem*, vol. 279, pp. 44294-302, Oct 2004.

[25] K. Hamamura, *et al.*, "Involvement of p38 MAPK in regulation of MMP13 mRNA in chondrocytes in response to surviving stress to endoplasmic reticulum," *Arch Oral Biol*, vol. 54, pp. 279-86, Mar 2009.

[26] D. Wang, *et al.*, "Isolation and characterization of MC3T3-E1 preosteoblast subclones with distinct *in vitro* and *in vivo* differentiation/mineralization potential," *J Bone Miner Res*, vol. 14, pp. 893-903, Jun 1999.

[27] Y. Li, *et al.*, "Mesenchymal stem/progenitor cells promote the reconstitution of exogenous hematopoietic stem cells in Fancg-/- mice *in vivo*," *Blood*, vol. 113, pp. 2342-51, Mar 2009.

[28] X. Wu, *et al.*, "Neurofibromin plays a critical role in modulating osteoblast differentiation of mesenchymal stem/progenitor cells," *Hum Mol Genet*, vol. 15, pp. 2837-45, Oct 2006.

[29] P. Zhang, *et al.*, "Diaphyseal bone formation in murine tibiae in response to knee loading," *J Appl Physiol*, vol. 100, pp. 1452-9, May 2006.

[30] G. N. Bancroft, *et al.*, "Fluid flow increases mineralized matrix deposition in 3D perfusion culture of marrow stromal osteoblasts in a dose-dependent manner," *Proc Natl Acad Sci U S A*, vol. 99, pp. 12600-5, Oct 2002.

[31] P. Ducy, *et al.*, "Osf2/Cbfa1: a transcriptional activator of osteoblast differentiation," *Cell*, vol. 89, pp. 747-54, May 1997.

[32] T. Komori, *et al.*, "Targeted disruption of Cbfa1 results in a complete lack of bone formation owing to maturational arrest of osteoblasts," *Cell*, vol. 89, pp. 755-64, May 1997.

[33] F. Otto, *et al.*, "Cbfa1, a candidate gene for cleidocranial dysplasia syndrome, is essential for osteoblast differentiation and bone development," *Cell*, vol. 89, pp. 765-71, May 1997.

[34] X. Yang, *et al.*, "ATF4 is a substrate of RSK2 and an essential regulator of osteoblast biology; implication for Coffin-Lowry Syndrome," *Cell*, vol. 117, pp. 387-98, Apr 2004.

[35] K. Nakashima, *et al.*, "The novel zinc finger-containing transcription factor osterix is required for osteoblast differentiation and bone formation," *Cell*, vol. 108, pp. 17-29, Jan 2002.

[36] T. Moroy and C. Geisen, "Cyclin E," *Int J Biochem Cell Biol*, vol. 36, pp. 1424-39, Aug 2004.

[37] P. Khatri, *et al.*, "Recent additions and improvements to the Onto-Tools," *Nucleic Acids Res*, vol. 33, pp. W762-5, Jul 2005.

[38] S. Draghici, *et al.*, "A systems biology approach for pathway level analysis," *Genome Res*, vol. 17, pp. 1537-45, Oct 2007.

[39] G. Wang, *et al.*, "Transcription factor and microRNA regulation in androgen-dependent and -independent prostate cancer cells," *BMC Genomics*, vol. 9 Suppl 2, p. S22, Sep 2008.

[40] P. Bhat-Nakshatri, *et al.*, "AKT alters genome-wide estrogen receptor alpha binding and impacts estrogen signaling in breast cancer," *Mol Cell Biol*, vol. 28, pp. 7487-503, Dec 2008.

[41] I. Kanazawa, *et al.*, "Adiponectin and AMP kinase activator stimulate proliferation, differentiation, and mineralization of osteoblastic MC3T3-E1 cells," *BMC Cell Biol*, vol. 8, p. 51, Nov 2007.

[42] F. Freitas, *et al.*, "Fluoroaluminate stimulates phosphorylation of p130 Cas and Fak and increases attachment and spreading of preosteoblastic MC3T3-E1 cells," *Bone*, vol. 30, pp. 99-108, Jan 2002.

[43] H. M. Zhang, *et al.*, "Coxsackievirus B3 Infection Activates the Unfolded Protein Response and Induces Apoptosis through Downregulation of p58IPK and Activation of CHOP and SREBP1," *J Virol*, Jun 2010.

[44] D. Ron and P. Walter, "Signal integration in the endoplasmic reticulum unfolded protein response," *Nat Rev Mol Cell Biol*, vol. 8, pp. 519-29, Jul 2007.

[45] S. Laing, *et al.*, "Airborne Particulate Matter Selectively Activates Endoplasmic Reticulum Stress Response in the Lung and Liver Tissues," *Am J Physiol Cell Physiol*, Jun 2010.

[46] S. J. Marciniak, *et al.*, "CHOP induces death by promoting protein synthesis and oxidation in the stressed endoplasmic reticulum," *Genes Dev*, vol. 18, pp. 3066-77, Dec 2004.

[47] H. P. Harding, *et al.*, "Regulated translation initiation controls stress-induced gene expression in mammalian cells," *Mol Cell*, vol. 6, pp. 1099-108, Nov 2000.

[48] H. Y. Jiang, *et al.*, "Activating transcription factor 3 is integral to the eukaryotic initiation factor 2 kinase stress response," *Mol Cell Biol*, vol. 24, pp. 1365-77, Feb 2004.

[49] K. M. Vattem and R. C. Wek, "Reinitiation involving upstream ORFs regulates ATF4 mRNA translation in mammalian cells," *Proc Natl Acad Sci U S A*, vol. 101, pp. 11269-74, Aug 2004.

[50] S. Oyadomari and M. Mori, "Roles of CHOP/GADD153 in endoplasmic reticulum stress," *Cell Death Differ*, vol. 11, pp. 381-9, Apr 2004.

[51] P. Zhang, *et al.*, "The PERK eukaryotic initiation factor 2 alpha kinase is required for the development of the skeletal system, postnatal growth, and the function and viability of the pancreas," *Mol Cell Biol*, vol. 22, pp. 3864-74, Jun 2002.

[52] M. Almeida, *et al.*, "Wnt proteins prevent apoptosis of both uncommitted osteoblast progenitors and differentiated osteoblasts by beta-catenin-dependent and -independent signaling cascades involving Src/ERK and phosphatidylinositol 3-kinase/AKT," *J Biol Chem*, vol. 280, pp. 41342-51, Dec 2005.

[53] P. Zhang, *et al.*, "Joint loading-driven bone formation and signaling pathways predicted from genome-wide expression profiles," *Bone*, vol. 44, pp. 989-98, May 2009.

[54] T. Bellido, *et al.*, "Activation of the Janus kinase/STAT (signal transducer and activator of transcription) signal transduction pathway by interleukin-6-type cytokines promotes osteoblast differentiation," *Endocrinology*, vol. 138, pp. 3666-76, Sep 1997.

[55] Y. Deyama, *et al.*, "Inactivation of NF-kappaB involved in osteoblast development through interleukin-6," *Biochem Biophys Res Commun*, vol. 282, pp. 1080-4, Apr 2001.

[56] S. Kinoshita, *et al.*, "Three-dimensional collagen gel culture promotes osteoblastic phenotype in bone marrow derived cells," *Kobe J Med Sci*, vol. 45, pp. 201-11, Oct 1999.

[57] I. Ishii, *et al.*, "Histological and functional analysis of vascular smooth muscle cells in a novel culture system with honeycomb-like structure," *Atherosclerosis*, vol. 158, pp. 377-84, Oct 2001.

[58] N. Boutahar, *et al.*, "Mechanical strain on osteoblasts activates autophosphorylation of focal adhesion kinase and proline-rich tyrosine kinase 2 tyrosine sites involved in ERK activation," *J Biol Chem*, vol. 279, pp. 30588-99, Jul 2004.

[59] N. Datta, *et al.*, "*In vitro* generated extracellular matrix and fluid shear stress synergistically enhance 3D osteoblastic differentiation," *Proc Natl Acad Sci U S A*, vol. 103, pp. 2488-93, Feb 2006.

[60] X. Wang, *et al.*, "p38 mitogen-activated protein kinase regulates osteoblast differentiation through osterix," *Endocrinology*, vol. 148, pp. 1629-37, Apr 2007.